

Exposing Backdoors in Robust Machine Learning Models

Ezekiel Soremekun^{*1} Sakshi Udeshi^{*2} Sudipta Chattopadhyay² Andreas Zeller¹

^{*}Equal contribution

Abstract

The introduction of robust optimisation has pushed the state-of-the-art in defending against adversarial attacks. However, the behaviour of such optimisation has not been studied in the light of a fundamentally different class of attacks called backdoors. In this paper, we demonstrate that adversarially robust models are susceptible to backdoor attacks. Subsequently, we observe that backdoors are reflected in the feature representation of such models. Then, this is leveraged to detect backdoor-infected models. Specifically, we use feature clustering to effectively detect backdoor-infected robust Deep Neural Networks (DNNs).

In our evaluation of major classification tasks, our approach effectively detects robust DNNs infected with backdoors. Our investigation reveals that salient features of adversarially robust DNNs break the stealthy nature of backdoor attacks.

1. Introduction

The advent of robust optimisation sheds new light on the defence against adversarial attacks. Specifically, if a machine learning (ML) model was trained with robust optimisation, then such a model is shown to be resilient against adversarial inputs (Madry et al., 2018) and we refer to such a model as a *robust model*. These adversarial inputs are intentionally crafted by attackers to cause an ML model to make wrong predictions. Although adversarially robust ML models are believed to be resilient against adversarial attacks, their susceptibility to other attack vectors is unknown. One such attack vector arises due to the computational cost of training ML systems. Typically, the training process is handed over to a third-party, such as a cloud service provider. Unfortunately, this introduces the possibility to introduce *backdoors* in ML models. The basic idea behind backdoors is to poison the training data and to train an ML algorithm with

the poisoned training data. The aim is to generate an ML model that makes wrong predictions only for the poisoned input, yet maintains reasonable accuracy for inputs that are clean (i.e. not poisoned). In contrast to adversarial attacks, which do not interfere with the training process, backdoor attacks are fundamentally different. Therefore, it is critical to investigate the impact of backdoor attacks and related defences for adversarially robust ML models.

In this paper, we carefully investigate backdoor attacks for adversarially robust models. We demonstrate that adversarially robust ML models can be infected with backdoors and such backdoor-infected models result in high attack success rates. Then, we develop a systematic methodology to detect backdoor-infected robust models. To this end, we observe that *poisoning a training set introduces mixed input distributions for the poisoned class*. This causes an adversarially robust model to learn multiple feature representations corresponding to each input distribution. In contrast, from a clean training data, an adversarially robust model learns only one feature representation for a particular prediction class (Santurkar et al., 2019). Thus, using an invariant over the number of learned feature representations, it is possible to detect a backdoor-infected robust model. We leverage feature clustering to check this invariant and detect backdoor-infected models.

In contrast to existing works on backdoor attacks and defence for ML models (Chen et al., 2019; Gu et al., 2017; Tran et al., 2018; Udeshi et al., 2019; Wang et al., 2019), in this paper, for the first time, we investigate backdoors in the context of adversarially robust ML models. Moreover, our proposed defence is completely automatic, unlike some defence against backdoors (Tran et al., 2018) our solution does not require any access to the poisoned data.

After discussing the prior work (Section 2) and providing an overview (Section 3), we make the following contributions:

1. We discuss the process of injecting two major backdoors (namely localised and distributed) during the training of an adversarially robust model (Section 4).
2. We show an invariant for checking the backdoor-infected models. We then leverage such an invariant via t-Distributed Stochastic Neighbor Embedding (t-SNE) and Mean shift clustering to detect backdoor-infected

¹CISPA – Helmholtz Center for Information Security

²Singapore University of Technology and Design. Correspondence to: Sakshi Udeshi <sakshi_udeshi@mymail.sutd.edu.sg>.

models (Section 4).

3. We evaluate the attack success rate of injecting localised as well as distributed backdoor triggers to poison the training data for MNIST, Fashion-MNIST and CIFAR-10. Our evaluation reveals an average attack success rate of 96% (Section 5).
4. We evaluate our defence on backdoor-infected models trained on three datasets. Our evaluation shows that the defence is accurate in detecting backdoor-infected models and it exposes the stealthy nature of backdoor attacks to users (Section 5).

After discussing some threats to validity (Section 6), we conclude in Section 7.

2. Related Work

Adversarial Robustness: Adversarial attacks for Neural Networks (NNs) were first introduced in (Szegedy et al., 2014). Researchers have introduced better adversarial attacks and built systems that are resilient to these attacks (He et al., 2017; Papernot et al., 2016a;b; 2017). A significant leap has been made by introducing robust optimisation to mitigate adversarial attacks (Madry et al., 2018; Raghu-nathan et al., 2018; Sinha et al., 2018; Wong & Kolter, 2018). These defences aim to guarantee the performance of machine learning models against adversarial examples. In this paper, we study the susceptibility of the models trained using robust optimisation to backdoor attacks. Then, we leverage the inherent properties of robust models to detect backdoor attacks.

Backdoor attacks: Backdoor attacks were introduced in BadNets (Gu et al., 2017), where an attacker poisons the training data by augmenting it. A pre-defined random shape is chosen for the attack. TrojanNN (Liu et al., 2018b) improves the attack by engineering the trigger and reducing the number of examples needed to insert the backdoor. Yao et al. (2019) propose a transfer learning based backdoor attack. All of these attacks were demonstrated for standard DNNs. To the best of our knowledge, we are the first to demonstrate the susceptibility of models trained under robust optimisation conditions (Madry et al., 2018) to backdoor attacks.

Backdoor Detection and Mitigation: Several approaches have been developed to detect backdoors in standard machine learning (ML). Tran et al. (2018) employ robust statistics to identify the inputs which are poisoned and sanitise the training data. Liu et al. (2018a) mitigate backdoor attacks by pruning neurons which behave maliciously, thus removing the neurons responsible for the backdoors. Chen et al. (2019) use the feature representations of the training and poisoned data to detect the poisoned data. Udeshi et al. (2019) propose a blackbox technique for the detection and

mitigation of backdoor attacks. None of these techniques mitigate backdoors in robust models. Wang et al. (2019) propose a white-box technique to mitigate backdoors in DNNs. This technique relies on finding a fixed perturbation that misclassifies a large set of inputs, but since robust models are designed to be resilient to exactly such perturbations, this technique would be inapplicable for robust models. Unlike the aforementioned works, we rely on the *clustering of feature representations in robust models* to detect backdoor attacks. Like our approach, Chen et al. (2019) employs feature clustering to detect backdoors in standard DNNs. However, their approach relies on *the strong assumption that the user has access to both the training dataset and the poisoned dataset*. Our approach requires access to only the model and the training dataset.

3. Overview

Attack Model: We assume an attack model seen commonly in previous work BadNets (Gu et al., 2017) and Trojan Attacks (Liu et al., 2018b). Specifically, in such an attack model, the user has no control over the training process. As a result, the user hands over the training data to an untrusted third party along with the training process specifications. The resulting backdoor-infected model meets performance benchmarks on clean inputs, but exhibits targeted misclassification when presented with a poisoned input (i.e. an input with an attacker defined backdoor trigger).

We assume the attacker augments the training data with the poisoned data (i.e. inputs with wrong labels) and then trains the model. This attack model is much stronger than the attack models considered in recent works (Du et al., 2019; Tran et al., 2018). Specifically, in contrast to the attack model considered in this paper, these works assume control over the training process (and additionally access to the clean training data). Nonetheless, as our work revolves around the investigation of robust DNNs, we do require the model to be trained under robust optimisation conditions. We note that it is possible to check whether a model is robust (Madry et al., 2018).

In addition, we assume for the targeted class, that poisoned inputs form an input distribution that is distinct from the distribution of the clean (training) images, this is in line with previous works (Gu et al., 2017; Liu et al., 2018b).

Backdoor detection in robust models: It has been observed by Santurkar et al. (2019) and Tsipras et al. (2019) that the images generated (by translation) for a robust model for a particular class align perceptually with the images of the class. This property is unique to robust classifiers. The images seen in Figure 1 are generated by a single CIFAR-10 classification model using first order methods, such as projected gradient descent based adversarial attacks (Madry

et al., 2018). This result is achieved by simply maximising the probability of the translated images to be classified under the targeted class (cf. Figure 1).

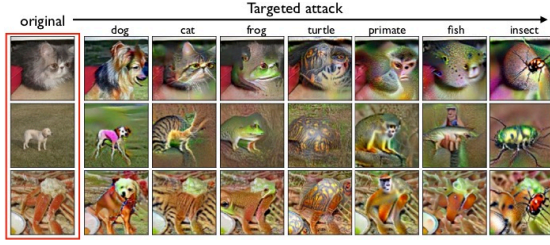


Figure 1. Image Translation using a robust model. This figure was taken from (Santurkar et al., 2019)

Key Insight: If there exists a mixture of distributions in the training dataset, for a particular class, then the model will learn multiple distributions. Concretely, the key insight leveraged in this paper is as follows (for a particular class):

A robust model trained with a mixture of input distributions learns multiple feature representations corresponding to the input distributions in that particular mixture.

In this paper, we visualise the aforementioned insight in two ways. First order methods (e.g. projected gradient descent based adversarial attacks (Madry et al., 2018)) are used to generate a set of inputs $X_{y^{(i)}}$ of a particular class with label $y^{(i)}$. Let us assume these inputs are generated (by translation) via a model that has been trained using a mixture distribution containing multiple input distributions in a class with label $y^{(i)}$. Then, multiple types of inputs will be observed in the generated inputs $X_{y^{(i)}}$. Such types of inputs should correspond to the different distributions in the mixture distribution for the class with label $y^{(i)}$. Consequently, if we visualise the feature representations of the generated inputs $X_{y^{(i)}}$, then we should observe that the feature representations are distinct corresponding to the distinct distributions in the mixture distribution for the class with label $y^{(i)}$.

Formalising the insight: Let f be a robust classifier that we train. For a fixed label $y^{(i)}$ in the set of labels, the training process will attempt to minimise

$$\mathbb{E}_{x \sim \mathcal{D}} \left[\max_{\delta \in \Delta} \mathcal{L}(x + \delta, y^{(i)}) \right] \quad (1)$$

Here, for a fixed label $y^{(i)}$ and loss function \mathcal{L} , the corresponding training data x is drawn from the mixture of distributions $\mathcal{D} = \sum_{i=0}^n \mathcal{D}_i$. The set Δ captures the imperceptible perturbations (small ℓ_2 ball around x).

Let us assume we attempt to generate a set of samples $X'_{y^{(i)}}$ for the class with label $y^{(i)}$ using the classifier f . We first

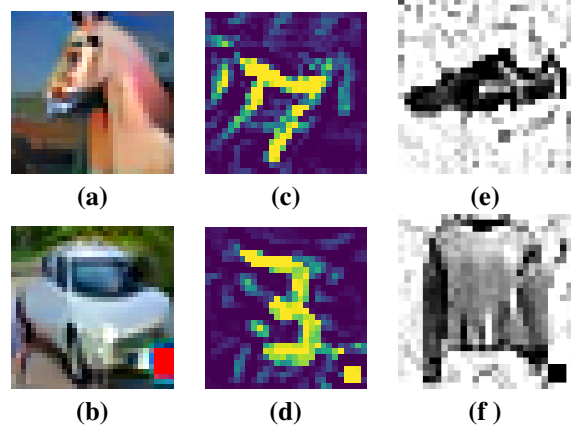


Figure 2. Translated images generated from mixed distributions by backdoor-infected robust model for the class *Horse* (a-b), 7 (c-d) and *Sneaker* (e-f). These are the target classes in the backdoor attack.

take an appropriate seed distribution \mathcal{G}_y . Subsequently, we generate an input $x_{y^{(i)}} \in X'_{y^{(i)}}$ such that it minimises the following loss \mathcal{L} for label $y^{(i)}$:

$$x_{y^{(i)}} = \arg \min_{||x' - x_0||_2 \leq \epsilon} \mathcal{L}(x', y^{(i)}), \quad x_0 \sim \mathcal{G}_y \quad (2)$$

We posit that the set $X'_{y^{(i)}}$ will contain generated inputs that belong to each distribution $\mathcal{D}_0, \mathcal{D}_1, \dots, \mathcal{D}_n$, which is part of the mixture of distributions \mathcal{D} .

Visualising the insight: To visualise this insight, we present Figure 2. The images shown in Figure 2 were generated via a model by taking random images from the corresponding dataset: CIFAR-10 for Figure 2 (a-b), MNIST digit for Figure 2 (c-d) and Fashion-MNIST for Figure 2 (f-g). This model was trained under robust optimisation conditions with poisoned training data to infect the model with backdoors. Random training data images are used to generate images of the target class in a robust backdoor-infected classifier. The classes are *Horse* in CIFAR-10, the digit 7 in MNIST-digit and the class *Sneaker* in Fashion-MNIST.

We observe the features that are maximised in Figure 2 (a, c, e) correspond to the actual classes. Whereas the counterparts seen in Figure 2 (b, d, f) correspond to the backdoor trigger (the small square at the bottom right corner of the image) used during training. We note that all images shown in Figure 2 were generated via the first order methods, as described in (Santurkar et al., 2019), only on a backdoor-infected robust model. This led us to observe both types of images (i.e. perceptually aligned and poisoned).

In addition to the aforementioned insight, the feature representations of the poisoned images form clusters that are distinct from the clusters of feature representations of clean images (Chen et al., 2019). However, such a detection method can only work when the user has access to both the

clean and the poisoned data set. Interestingly, we observe that the set of translated images, for a backdoor-infected robust model, contain both the clean (training) images and poisoned images. Thus, the feature representations of these images form different clusters. We use this to automate the detection of classes with a backdoor, without access to the poisoned images or the training process.

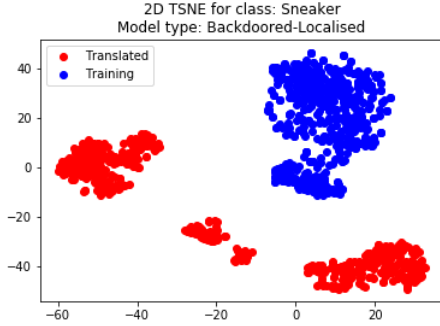


Figure 3. Feature representations of translated images and training images (for the class *Sneaker*) for a poisoned Fashion-MNIST classifier

Figure 3 captures the feature representations of a backdoor-infected robust model. The feature representations are the outputs of the last hidden layer of a DNN. We reduce the dimensions of the feature representations and visualise them using t-SNE (Maaten & Hinton, 2008). In this case, we trained a robust network with a backdoor and the feature representations in Figure 3 belong to the target class (*Sneaker*). The images for this class (as generated via translation) have multiple feature representations (i.e. using projected gradient descent based adversarial attacks (Madry et al., 2018)). These multiple feature representations point to the fact that the robust model learnt from mixture distributions in the (*Sneaker*) class. Thus, a quick check of the translated images reveals two types of images – one corresponding to the actual class *Sneaker* and one to the backdoor as seen in Figure 2 (e-f).

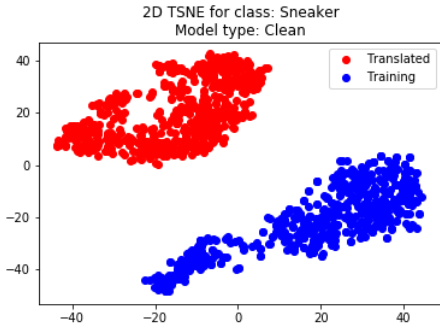


Figure 4. Feature representations of translated images and training images (for the class *Sneaker*) for an unpoisoned Fashion-MNIST classifier

In contrast, Figure 4 captures the feature representations

of a clean, yet robust model. The feature representations of the translated images for class *Sneaker* form only one cluster. This is expected behaviour, because the clean model learns only one distribution in *Sneaker* class. Consequently, the translated images also form only one representation that maximises the probability to be categorised in *Sneaker* class.

We observe, there are two clusters for every untargeted or clean class, specifically, the training set cluster and the translated image cluster. The translated images form a different cluster from the training set because they maximise the class probability of the training images. As a result they exaggerate the feature representations of the training set most effectively (Santurkar et al., 2019). This phenomenon leads to the translated images forming a separate cluster.

Feature Clustering: We automate the detection of clusters of feature representations by leveraging the mean shift clustering algorithm (Fukunaga & Hostetler, 1975). An example of applying mean shift can be seen in Figure 5, where the mean shift algorithm predicts three classes for the translated images, as generated by a backdoor-infected robust model. We further investigated the content inside these clusters by checking the images associated with the feature representations that make up these clusters. Specifically, the purple cluster (cf. Figure 5) contained inputs seen in Figure 6(a). These are the translated inputs which exhibit the backdoor. In contrast, the inputs seen in the yellow cluster (cf. Figure 5) contained translated images seen in Figure 6(b). These images correspond to the features of the actual training images in class *Sneaker*.

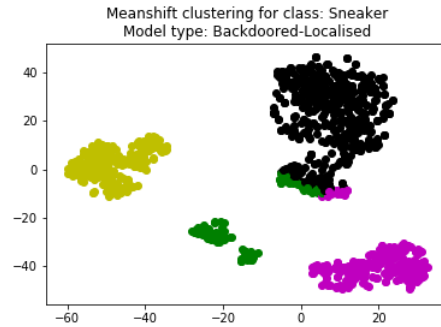


Figure 5. Mean shift clustering of the feature representations of translated images and training images (for the class *Sneaker*) for a poisoned Fashion-MNIST classifier

4. Detailed Methodology

Backdoor Injection: We show that despite being highly resilient to known adversarial attacks (Madry et al., 2018), robust backdoor models are still susceptible to backdoor attacks. It takes very few poisoned training images (as little as 1%) for the backdoor to be successfully injected. We use

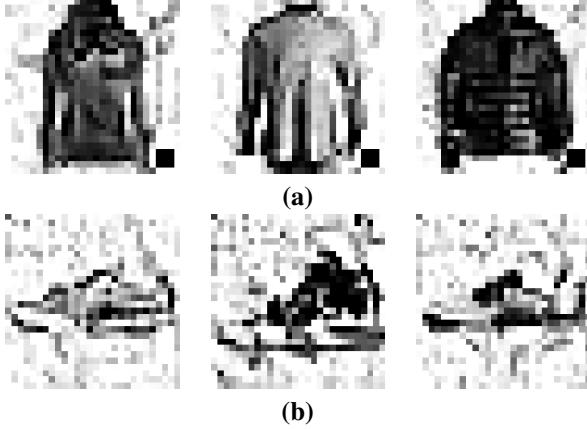


Figure 6. Inputs in the clusters seen in Figure 5. The purple cluster contains inputs seen in (a), where as the yellow cluster represents contains inputs seen in (b). It is important to note that these images were generated in the same instantiation of the projected gradient descent based adversarial attacks (Madry et al., 2018).

backdoor injection techniques similar to the one seen in Gu et al. (2017). We randomly select and poison one percent of the training images at random from each dataset (e.g. 500 images for CIFAR-10). We poison these images by adding the respective backdoor trigger (localised or distributed) to the images and augment them to the training data. Once this modified dataset is ready, we train the model using this data.

Backdoored Model Detection: In this section, we elucidate the methodologies behind our detection technique in detail. We only assume white-box access to the model and access to the training data. In Table 1, we introduce some notation to help us illustrate our approach.

Table 1. Notations used in our approach

f	The robust machine learning classifier under test.
Y	Set of labels for f
\mathbb{D}	The full training data
\mathcal{L}	The loss function
$\mathcal{R}(\cdot)$	A function that returns the feature representation flattened to single 1D vector
$X_{y^{(i)}}$	Vector of training data points for label $y^{(i)} \in Y$
$X'_{y^{(i)}}$	Vector of translated data points for label $y^{(i)} \in Y$

Backdoor detection: First we provide a high level overview of the defence before going into each step in detail. Typically, the data points of a particular class follow a single distribution and as a result, form only one cluster after undergoing t-SNE (Maaten & Hinton, 2008). However, when a backdoor attack is carried out, the adversary inadvertently injects a mixture of distributions in one class, resulting in more than one cluster. The identification of a mixture distribution in a class is the main intuition behind our approach.

Algorithm 1 Backdoor Detection

Input: Robust ML classifier f , Sample of training data points X , Sample of translated data points X' , bandwidth for the mean shift algorithm b

for $y^{(i)} \in Y$ **do**

$$R_{X_{y^{(i)}}} = \mathcal{R}(f, X_{y^{(i)}})$$

$$R_{X'_{y^{(i)}}} = \mathcal{R}(f, X'_{y^{(i)}})$$

$$R_{y^{(i)}} = \text{concatenate}(R_{X_{y^{(i)}}}, R_{X'_{y^{(i)}}})$$

\triangleright *tsne* reduces the feature dimensions

$$\hat{R}_{y^{(i)}} = \text{tsne}(R_{y^{(i)}}), b)$$

$$\text{predicted_classes} = \text{meanshift}(\hat{R}_{y^{(i)}})$$

$$\text{analyseForBackdoor}(\hat{R}_{y^{(i)}}, \text{predicted_classes})$$

end for

The hypothesis is that the image generation process for robust models, as seen in Santurkar et al. (2019), will follow similar distributions as the training data. Since the target class in a backdoor model will be learning from multiple distributions, there will be multiple distributions of feature representation of the translated images (generated via first order adversarial methods). Our aim is to detect these multiple feature distributions. To detect such multiple distributions, we leverage t-SNE and Mean shift clustering.

For each label $y^{(i)} \in Y$, Algorithm 1 generates translated images via first order-based adversarial methods (Step 1). Then, it extracts the feature representations from the training and translated images for the label $y^{(i)}$ (Step 2). Next, the dimensions of the extracted features are reduced using t-SNE (Step 3). Mean shift is then employed to calculate the number of clusters in the reduced feature representations (Step 4). Finally, the number of resulting clusters is used to flag the backdoor-infected model (and poisoned class) as suspicious, if necessary (Step 5).

Step 1 - Image Translation: To effectively analyse a model for backdoors, a vector of translated images $X'_{y^{(i)}}$ where $y^{(i)} \in Y$ needs to be built. In robust classifiers, image translation leads to perceptually aligned images (Santurkar et al., 2019). This image translation is done for all $y^{(i)} \in Y$. The following function is minimised (and the probability of the target class $y^{(i)}$ is maximised):

$$x = \arg \min_{\|x' - x_0\|_2 \leq \epsilon} \mathcal{L}(x', y^{(i)}), \quad x_0 \in \mathbb{D} \quad (3)$$

The algorithm samples a seed from the training data \mathbb{D} and minimises the loss \mathcal{L} of the particular label $y^{(i)}$ to generate the translated images. This is done across 500 random seed images to obtain $X'_{y^{(i)}}$.

Step 2 - Feature Representations: Since our technique relies on the feature representations of the images, the al-

gorithm now extracts them using $X_{y^{(i)}}$ and $X'_{y^{(i)}}$ for $y^{(i)} \in Y$. We define $\mathcal{R}(\cdot)$ as a function that maps an input x to a vector $\mathcal{R}(x, f)$ in the representation (penultimate layer) for a robust model f .

Once $X_{y^{(i)}}$ and $X'_{y^{(i)}}$ are generated for $y^{(i)} \in Y$, the algorithm runs a forward pass of all the inputs $x \in X_{y^{(i)}}$ and $x' \in X'_{y^{(i)}}$ through the robust model f . The algorithm extracts the outputs of the last hidden layer and flattens them to form feature representations $R_{X_{y^{(i)}}}$ and $R_{X'_{y^{(i)}}}$, for $X_{y^{(i)}}$ and $X'_{y^{(i)}}$, respectively. These feature representations concatenated into $R_{y^{(i)}}$ for all $y^{(i)} \in Y$.

Step 3 - t-SNE: t-distributed stochastic neighbour embedding (t-SNE) is a data visualisation technique first introduced in [Maaten & Hinton \(2008\)](#). It is a nonlinear dimensionality reduction algorithm, which is primarily used to visualise high dimensional data in a two or three dimensional space. t-SNE is used to visualise the feature representations $R_{y^{(i)}}$ for all $y^{(i)} \in Y$ and to reduce their dimension. This is done to find any unusual clustering in the translated images. As expected, there are multiple clusters of feature representations in the target class of a backdoored model. As seen in Figure 3 for a target class, the feature representations of the translated images show two clusters. This is because the learning process had inputs from two distributions (i.e. clean inputs and poisoned inputs). This phenomenon was also observed in [Tran et al. \(2018\)](#).

Step 4 - Mean shift: To further automate the process of detection, the mean shift algorithm ([Fukunaga & Hostetler, 1975](#)) is leveraged. This is a clustering algorithm which is used to identify the clusters automatically. Mean shift tries to locate the modes of a density function. It does this by trying to discover "blobs" in a smooth density of samples. It updates candidates for centroids to be a mean of points in a given region and then eliminates duplicates to form a final set of points ([Fukunaga & Hostetler, 1975](#)). One can see in Figure 5 that the algorithm identifies four classes.

Step 5 - Detection: After the mean shift, all the classes that show multiple distributions in the translated images are flagged as suspicious. A user can examine the examples in the cluster as seen in Figure 6. This helps the user to inspect if there is indeed a backdoor in the image and the model was poisoned.

5. Experimental Results

In this section, we describe the experimental setup and the results for the backdoor injection attack and the proposed detection technique, using three major classification tasks.

Research questions: We evaluate the success rate of backdoor injection attacks on adversarially robust models and the effectiveness of our detection technique. In particular,

Image Type	Dataset (#labels)	Arch.	Input Size	# of Images training	# of Images test
Objects	CIFAR-10 (10)	ResNet50	32 x 32 x 3	50,000	10,000
Digits	MNIST (10)	ResNet18	28 x 28 x 1	60,000	10,000
Fashion Article	Fashion-MNIST (10)	ResNet18	28 x 28 x 1	60,000	10,000

Table 2. Dataset details and complexity of the classification tasks

Detection Parameters	All Models		
	MNIST	Fashion-MNIST	CIFAR-10
Epsilon (ϵ)	100	100	500
t-SNE Perplexity	30	30	30
Mean shift Bandwidth	35	28	21

Table 3. Backdoor Detection Parameters

we ask the following research questions:

- **RQ1 Attack Success Rate.** How effective is backdoor injection attacks on adversarially robust models?
- **RQ2 Detection Effectiveness.** How effective is the proposed detection approach?
- **RQ3 Attack Comparison.** What is the comparative performance of localised and distributed backdoors, in terms of attack success rate and detection?

Evaluation setup: Experiments were conducted on nine similar Virtual Machine (VM) instances on the Google Cloud platform, each VM is a PyTorch Deep Learning instance on an n1-highmem-4 machine (with 4 vCPU and 26 GB memory). Each VM had an Intel Broadwell CPU platform, 1 X NVIDIA Tesla GPU with eight to 16GB GPU memory and a 100 GB standard persistent disk.

Datasets, Models and Adversarial Training: For our experiments, we use the CIFAR-10 ([Krizhevsky et al., 2009](#)), MNIST ([LeCun et al., 1998](#)) and Fashion-MNIST ([Xiao et al., 2017](#)) datasets. MNIST and Fashion-MNIST have 60,000 training images each, while CIFAR-10 has 50,000 training images (cf. Table 2). Each dataset has 10 classes and 10,000 test images. MNIST and Fashion-MNIST experiments were trained with the standard ResNet-18 architecture, while CIFAR-10 was trained using the standard ResNet-50 architecture ([He et al., 2016](#)). Only CIFAR-10 models were trained with data augmentation, with momentum of 0.9 and weight decay of $5e^{-4}$. We trained all robust classifiers using the adversarial training methodology of ([Madry et al., 2018](#)) with an l_2 perturbation set. All experiments were conducted with the default hyperparameters in the robustness package ([Engstrom et al., 2019](#)).

Attack Configuration: We employed the backdoor data poisoning approach outlined in BadNets ([Gu et al., 2017](#)) to inject backdoors during adversarial training for all datasets. For infected models and all datasets, we created a set of backdoor infected images by modifying a portion of the

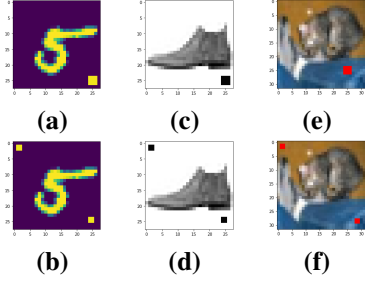


Figure 7. Triggers for MNIST (a) localised and (b) distributed backdoors, Fashion-MNIST (c) localised and (d) distributed backdoors and CIFAR-10 (e) localised and (f) distributed backdoors

Dataset	Backdoor-Infected Models Attack Success Rate (Classification accuracy)		Clean Model
	Localised	Distributed	
CIFAR-10	82.58 (89.80)	99.85 (90.22)	90.28
MNIST	99.96 (99.59)	100.00 (99.53)	99.61
Fashion-MNIST	96.26 (91.83)	99.77 (91.80)	91.99

Table 4. Backdoor attack success rate and classification accuracy

training datasets, specifically we apply a trigger to one percent of the clean images in the training set (e.g. 600 images for the MNIST dataset). Additionally, we modify the class label of each poisoned image to class seven for all datasets and all attack types, then we train DNN models with the modified training data to 100 epochs for Fashion-MNIST and MNIST, and 110 epochs for CIFAR-10.

The triggers for each attack and tasks are shown in Figure 7. The trigger for localised backdoors is a square at the bottom right corner of the image, this is to avoid covering the important parts of the original training image. The trigger for distributed backdoors is made up of two smaller squares, one at the top left corner of the image and another at the bottom right corner. The total size of the trigger is less than one percent of the entire image for both attack types.

Detection Configuration: The detection configuration used in our evaluation are shown in Table 3. For each dataset, the epsilon (ϵ) ball for input perturbation is fixed. For MNIST and Fashion-MNIST, the parameter ϵ is 100 and it is 500 for CIFAR-10. This places a uniform limit on input perturbation for each dataset. The perplexity for t-SNE is a tuneable parameter that balances the attention between the local and global aspects of the data. The authors suggest a value between 5 and 50 (Maaten & Hinton, 2008) and as a result we chose 30. The bandwidth in the mean shift algorithm is the size of the kernel function. This value is constant for each dataset. The bandwidth is 35, 28 and 21 for MNIST, Fashion-MNIST and CIFAR-10 respectively.

Evaluation Metrics: We measure the performance of the backdoor injection attack by computing the *classification accuracy* on the testing data. We compute the *attack success rate* by applying the trigger to all test images and measuring the number of modified images that are classified to the

attack target label, i.e. classified to class seven. We also measure the classification accuracy of the clean adversarially robust models as a baseline for comparison. In addition, for detection efficacy, we report the *number of feature representation clusters* found for all classes of all robust models in our configuration.

RQ1 - Attack Success Rate: In this section, we present the effectiveness of the backdoor injection attack. We illustrate that backdoors can be effectively injected in robust models without significantly reducing the classification accuracy of the models.

In our evaluation, we found that robust models are highly vulnerable to backdoor attacks. Backdoors effectively caused the misclassification of 96.4% of backdoor-infected images to the attacker selected target labels, across all datasets and attack types. Specifically, on average, localised backdoors and distributed backdoors caused the misclassification of 92.93% and 99.87% of backdoor-infected images, respectively (cf. Table 4).

Robust DNNs are highly susceptible to backdoor attacks, with a 96.4% attack success rate, on average.

Backdoor injection in robust DNNs does not cause a significant reduction in the classification accuracy for clean images. Backdoor-infected models still achieved a high classification accuracy for clean images, 93.8% classification accuracy on average. In comparison, *clean robust models* achieved a 93.96% classification accuracy, this shows an insignificant reduction in accuracy of 0.18%. In particular, localised backdoors and distributed backdoors maintained a high classification accuracy of 93.74% and 93.85% on average, respectively (cf. Table 4).

Backdoor-infected models maintain a high classification accuracy on clean images (93.8% on average).

RQ2 - Detection Performance: In this section, we evaluate the efficacy of our backdoor detection approach. We demonstrate that the technique is effective in (a) detecting backdoor-infected robust models and (b) revealing the backdoor-infected class.

In our evaluation, our approach effectively detected all backdoor-infected robust DNNs, for both localised and distributed backdoors, for all classification tasks. It accurately detected all backdoor-infected models by identifying classes that have more than two feature clusters for the training set and the translated image set. The results showed that all clean untargeted classes of backdoor-infected robust models, as well as all classes of clean robust models have exactly two clusters, while, all targeted classes of backdoor-infected models have more than two clusters (cf. Table 5).

Class Type	Class Labels	MNIST Models			Fashion-MNIST Models			CIFAR-10 Models		
		Backdoor-Infected Local	Distributed	Clean	Backdoor-Infected Local	Distributed	Clean	Backdoor-Infected Local	Distributed	Clean
Targeted	{7}	3	3	2	4	3	2	3	4	2
Untargeted	{0 – 6, 8, 9}	2	2	2	2	2	2	2	2	2

Table 5. Detection Efficacy: Number of feature clusters for each class

In particular, for each targeted class, the mean shift clustering of the features of the backdoor-infected models reveals these models consistently have more than two clusters. Notably, these clusters include one cluster for the clean training images and at least two clusters for the translated images. The clusters for the translated images include at least one cluster capturing the image translation for the poisoned images, and another cluster for the translated clean images. Meanwhile, the clean untargeted classes have precisely two clusters of features, one for the training set and another for the translated image set. Likewise, for the clean robust models, each class has exactly two distinct clusters, one cluster for the training set and another cluster for the translated image set (*cf.* Table 5).

Our approach effectively detected all (100%) backdoor-infected robust DNNs.

Our detection approach accurately identified the infected class, for all classification tasks and both attack types (*cf.* Table 5). The mean shift feature clustering of each class in the backdoor-infected model reveals that only the infected class had more than two clusters, with one cluster for the training set and at least two clusters for the translated images.

Our approach identified the backdoor-infected class for all classification tasks.

RQ3 - Attack Comparison: In this section, we compare the performance of the two attack types, namely the localised and the distributed backdoor attack. Specifically, we compare the attack success rate, the classification accuracy and the detection efficacy for both attacks.

The distributed backdoor attack is more effective than the localised backdoor attack, it has a higher attack success rate. The distributed attack is 6.95% more successful than the localised attack, on average (*cf.* Table 4). Additionally, on average, the distributed backdoor attacks have a higher classification accuracy than the localised backdoor attacks, albeit only a slight improvement of 0.12%. Overall, the distributed backdoors performed better than the localised backdoors.

The distributed backdoor attack is (6.95%) more effective than the localised backdoor attack, on average.

In our evaluation, our approach effectively detects both attacks equally. Our detection technique is designed to be *attack agnostic*: It is effective regardless of the attack type (i.e. localise or distributed backdoors). In addition, regardless of the attack type, our approach detected the infected class (*cf.* Table 5).

Our detection approach is attack-agnostic: it detects backdoor-infected model, regardless of the attack type.

6. Threats to Validity

Our evaluation is limited to the following threats to validity:

External validity: This refers to the generalisability of our approach and results. We have evaluated our approach using three popular classification tasks, several adversarially robust models and two major attack types. However, there is a threat that our approach does not generalise to other classification tasks or backdoors. We have mitigated this threat by evaluating the performance of our approach using the two popular backdoor attack types found in the literature and three major classification tasks with varying levels of complexity. These classification tasks have thousands of training and test images, providing confidence that our approach will work on more complex tasks and models.

Construct validity: It is possible that advanced backdoor triggers can be crafted to align to the input distribution of the training dataset. We mitigate this threat by ensuring that our backdoor triggers are similar to the ones described in the literature, as reported in previous related research.

7. Conclusion

In this paper, we demonstrate a new attack vector for robust ML models, namely backdoor attacks. We show that robust models are susceptible to backdoors. Then, we leverage the inherent properties of robust ML models to detect such an attack. Our detection approach accurately detects backdoor-infected models and the poisoned class, without any access to the poisoned data. Our work reveals a major strength of robust optimisation in exposing backdoors. Our code and experimental data are available for replication:

<https://github.com/sakshiudeshi/Expose-Robust-Backdoors>

References

- Chen, B., Carvalho, W., Baracaldo, N., Ludwig, H., Edwards, B., Lee, T., Molloy, I., and Srivastava, B. Detecting backdoor attacks on deep neural networks by activation clustering. In *Workshop on Artificial Intelligence Safety 2019 co-located with the Thirty-Third AAAI Conference on Artificial Intelligence 2019 (AAAI-19)*, Honolulu, Hawaii, January 27, 2019, 2019.
- Du, M., Jia, R., and Song, D. Robust anomaly detection and backdoor attack detection via differential privacy. *CoRR*, abs/1911.07116, 2019. URL <http://arxiv.org/abs/1911.07116>.
- Engstrom, L., Ilyas, A., Santurkar, S., and Tsipras, D. Robustness (python library), 2019. URL <https://github.com/MadryLab/robustness>.
- Fukunaga, K. and Hostetler, L. D. The estimation of the gradient of a density function, with applications in pattern recognition. *IEEE Trans. Information Theory*, 21(1):32–40, 1975.
- Gu, T., Dolan-Gavitt, B., and Garg, S. Badnets: Identifying vulnerabilities in the machine learning model supply chain. *CoRR*, abs/1708.06733, 2017. URL <http://arxiv.org/abs/1708.06733>.
- He, K., Zhang, X., Ren, S., and Sun, J. Deep residual learning for image recognition. In *Proceedings of the IEEE conference on computer vision and pattern recognition*, pp. 770–778, 2016.
- He, W., Wei, J., Chen, X., Carlini, N., and Song, D. Adversarial example defense: Ensembles of weak defenses are not strong. In *11th USENIX Workshop on Offensive Technologies, WOOT 2017, Vancouver, BC, Canada, August 14-15, 2017*, 2017.
- Krizhevsky, A., Hinton, G., et al. Learning multiple layers of features from tiny images. 2009.
- LeCun, Y., Cortes, C., and Burges, C. J. The mnist database of handwritten digits, 1998. URL <http://yann.lecun.com/exdb/mnist>, 10:34, 1998.
- Liu, K., Dolan-Gavitt, B., and Garg, S. Fine-pruning: Defending against backdooring attacks on deep neural networks. In *Research in Attacks, Intrusions, and Defenses - 21st International Symposium, RAID 2018, Heraklion, Crete, Greece, September 10-12, 2018, Proceedings*, pp. 273–294, 2018a.
- Liu, Y., Ma, S., Aafer, Y., Lee, W.-C., Zhai, J., Wang, W., and Zhang, X. Trojaning attack on neural networks. In *25th Annual Network and Distributed System Security Symposium, NDSS 2018, San Diego, California, USA, February 18-22, 2018*. The Internet Society, 2018b.
- Maaten, L. v. d. and Hinton, G. Visualizing data using t-sne. *Journal of machine learning research*, 9(Nov): 2579–2605, 2008.
- Madry, A., Makelov, A., Schmidt, L., Tsipras, D., and Vladu, A. Towards deep learning models resistant to adversarial attacks. In *6th International Conference on Learning Representations, ICLR 2018, Vancouver, BC, Canada, April 30 - May 3, 2018, Conference Track Proceedings*, 2018.
- Papernot, N., McDaniel, P. D., Jha, S., Fredrikson, M., Celik, Z. B., and Swami, A. The limitations of deep learning in adversarial settings. In *IEEE European Symposium on Security and Privacy, EuroS&P 2016, Saarbrücken, Germany, March 21-24, 2016*, pp. 372–387, 2016a.
- Papernot, N., McDaniel, P. D., Wu, X., Jha, S., and Swami, A. Distillation as a defense to adversarial perturbations against deep neural networks. In *IEEE Symposium on Security and Privacy, SP 2016, San Jose, CA, USA, May 22-26, 2016*, pp. 582–597, 2016b.
- Papernot, N., McDaniel, P. D., Goodfellow, I. J., Jha, S., Celik, Z. B., and Swami, A. Practical black-box attacks against machine learning. In *Proceedings of the 2017 ACM on Asia Conference on Computer and Communications Security, AsiaCCS 2017, Abu Dhabi, United Arab Emirates, April 2-6, 2017*, pp. 506–519, 2017.
- Raghunathan, A., Steinhardt, J., and Liang, P. Certified defenses against adversarial examples. In *6th International Conference on Learning Representations, ICLR 2018, Vancouver, BC, Canada, April 30 - May 3, 2018, Conference Track Proceedings*, 2018. URL <https://openreview.net/forum?id=Bys4ob-Rb>.
- Santurkar, S., Ilyas, A., Tsipras, D., Engstrom, L., Tran, B., and Madry, A. Image synthesis with a single (robust) classifier. In *Advances in Neural Information Processing Systems 32: Annual Conference on Neural Information Processing Systems 2019, NeurIPS 2019, 8-14 December 2019, Vancouver, BC, Canada*, pp. 1260–1271, 2019.
- Sinha, A., Namkoong, H., and Duchi, J. C. Certifying some distributional robustness with principled adversarial training. In *6th International Conference on Learning Representations, ICLR 2018, Vancouver, BC, Canada, April 30 - May 3, 2018, Conference Track Proceedings*, 2018. URL <https://openreview.net/forum?id=Hk6kPgZA->.

- Szegedy, C., Zaremba, W., Sutskever, I., Bruna, J., Erhan, D., Goodfellow, I. J., and Fergus, R. Intriguing properties of neural networks. In *2nd International Conference on Learning Representations, ICLR 2014, Banff, AB, Canada, April 14-16, 2014, Conference Track Proceedings*, 2014.
- Tran, B., Li, J., and Madry, A. Spectral signatures in backdoor attacks. In *Advances in Neural Information Processing Systems 31: Annual Conference on Neural Information Processing Systems 2018, NeurIPS 2018, 3-8 December 2018, Montréal, Canada*, pp. 8011–8021, 2018.
- Tsipras, D., Santurkar, S., Engstrom, L., Turner, A., and Madry, A. Robustness may be at odds with accuracy. In *7th International Conference on Learning Representations, ICLR 2019, New Orleans, LA, USA, May 6-9, 2019*, 2019.
- Udeshi, S., Peng, S., Woo, G., Loh, L., Rawshan, L., and Chattopadhyay, S. Model agnostic defence against backdoor attacks in machine learning. *CoRR*, abs/1908.02203, 2019. URL <http://arxiv.org/abs/1908.02203>.
- Wang, B., Yao, Y., Shan, S., Li, H., Viswanath, B., Zheng, H., and Zhao, B. Y. Neural cleanse: Identifying and mitigating backdoor attacks in neural networks. In *2019 IEEE Symposium on Security and Privacy, SP 2019, Proceedings, 20-22 May 2019, San Francisco, California, USA*, 2019.
- Wong, E. and Kolter, J. Z. Provable defenses against adversarial examples via the convex outer adversarial polytope. In *Proceedings of the 35th International Conference on Machine Learning, ICML 2018, Stockholmsmässan, Stockholm, Sweden, July 10-15, 2018*, pp. 5283–5292, 2018. URL <http://proceedings.mlr.press/v80/wong18a.html>.
- Xiao, H., Rasul, K., and Vollgraf, R. Fashion-mnist: a novel image dataset for benchmarking machine learning algorithms, 2017.
- Yao, Y., Li, H., Zheng, H., and Zhao, B. Y. Latent backdoor attacks on deep neural networks. In *Proceedings of the 2019 ACM SIGSAC Conference on Computer and Communications Security, CCS 2019, London, UK, November 11-15, 2019*, pp. 2041–2055, 2019. doi: 10.1145/3319535.3354209. URL <https://doi.org/10.1145/3319535.3354209>.

Appendices

A. Experimental Setup

A.1. Datasets and Models

In our evaluation, we use three major datasets, namely CIFAR-10 (Krizhevsky et al., 2009), MNIST (LeCun et al., 1998) and Fashion-MNIST (Xiao et al., 2017). MNIST and Fashion-MNIST models were trained with the standard ResNet-18 architecture, while CIFAR-10 models were trained using the standard ResNet-50 architecture (He et al., 2016). All experiments were conducted with the default learning rate (LR) scheduling in the robustness package (Engstrom et al., 2019), i.e. the PyTorch StepLR optimisation scheduler. The learning rate is initially set to 0.1 for training (LR) and the scheduler decays the learning rate of each parameter group by 0.1 (gamma) every 50 epochs (default step size). All models were trained with momentum of 0.9 and weight decay of $5e^{-4}$. Only CIFAR-10 models were trained with data augmentation, this is the default configuration in the robustness package for CIFAR-10.

Dataset	Epochs	LR	Batch Size	LR Schedule
CIFAR-10	110	0.1	128	Drop by 10 at epochs $\in [50, 100]$
MNIST	100	0.1	128	Drop by 10 at epochs $\in [50, 100]$
Fashion-MNIST	100	0.1	128	Drop by 10 at epochs $\in [50, 100]$

Table 6. Standard Hyperparameters used for model training.

A.2. Adversarial Training

For our evaluation, all models were trained with robust optimisation based on the adversarial training approach of (Madry et al., 2018) with an l_2 perturbation set. The parameters for robust training are the same for all datasets. In particular, all models were trained with an adversarial attack budget of 0.5 (ϵ), and an attack step size of 1.5 (step size) and set to take 20 steps (# steps) during adversarial attack (cf. Table 7). All other hyperparameters are set to the default hyperparameters (cf. Table 7) in the robustness package (Engstrom et al., 2019). No hyperparameter tuning was performed for the adversarial training of models.

Dataset	ϵ	# steps	Step size
CIFAR-10	0.5	20	1.5
MNIST	0.5	20	1.5
Fashion-MNIST	0.5	20	1.5

Table 7. Hyperparameters used for adversarially robust model training and evaluation.

A.3. Adversarial Accuracy

Adversarial evaluation was performed with the same parameters as adversarial training for all datasets and models. In particular, all classifiers were evaluated with an adversarial attack budget of 0.5 (ϵ), and an attack step size of 1.5 and set to take 20 steps during adversarial attack (*cf.* Table 7). In addition, for adversarial evaluation, we use the best loss in PGD step as the attack ('use_best': True,), with no random restarts ('random_restarts': 0) and no fade in epsilon along epochs ('eps_fadein_epochs': 0). Overall, results showed that all models maintained a similarly high adversarial accuracy for both clean and backdoor-infected models (*cf.* Table 8). Specifically, 86.22% adversarial accuracy, on average. Hence, adversarial training accuracy is not inhibited by the backdoor attack vector.

Dataset	Adversarial Accuracy		
	Backdoor-Infected Models Localised	Backdoor-Infected Models Distributed	Clean Model
CIFAR-10	68.26	68.17	68.64
MNIST	99.51	99.49	99.55
Fashion-MNIST	90.78	90.66	90.91

Table 8. Adversarial accuracy of all robust classifiers.

B. Additional Figures

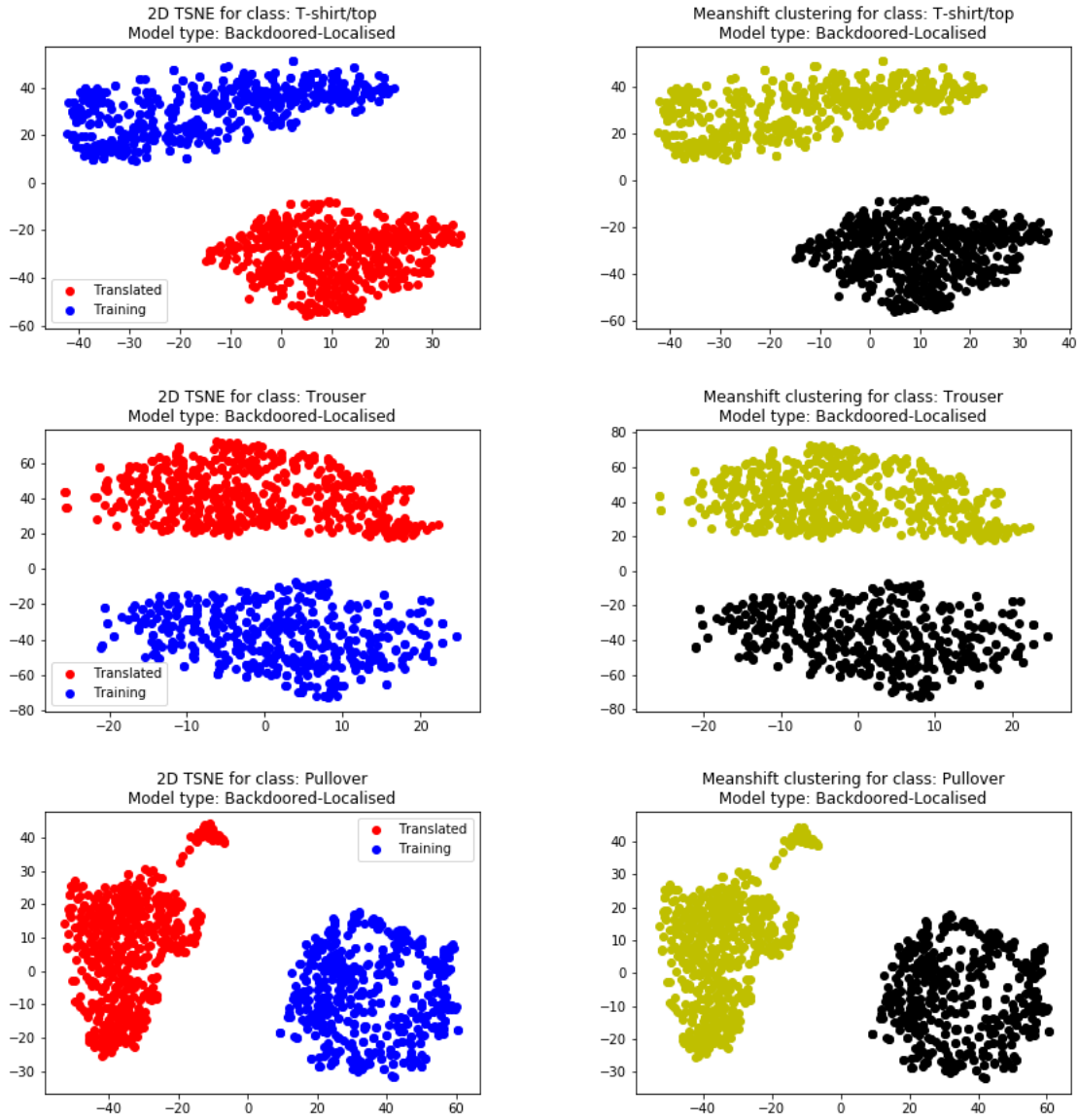


Figure 8. Feature representation clusters for backdoored Fashion-MNIST models (Localised) with target class *Sneaker* (7). Showing class 0 to 2 in this figure. The left column shows the feature representations of the translated and the training images, whereas the right column shows the result of the Mean shift clustering on the corresponding points where different colours represent different classes.

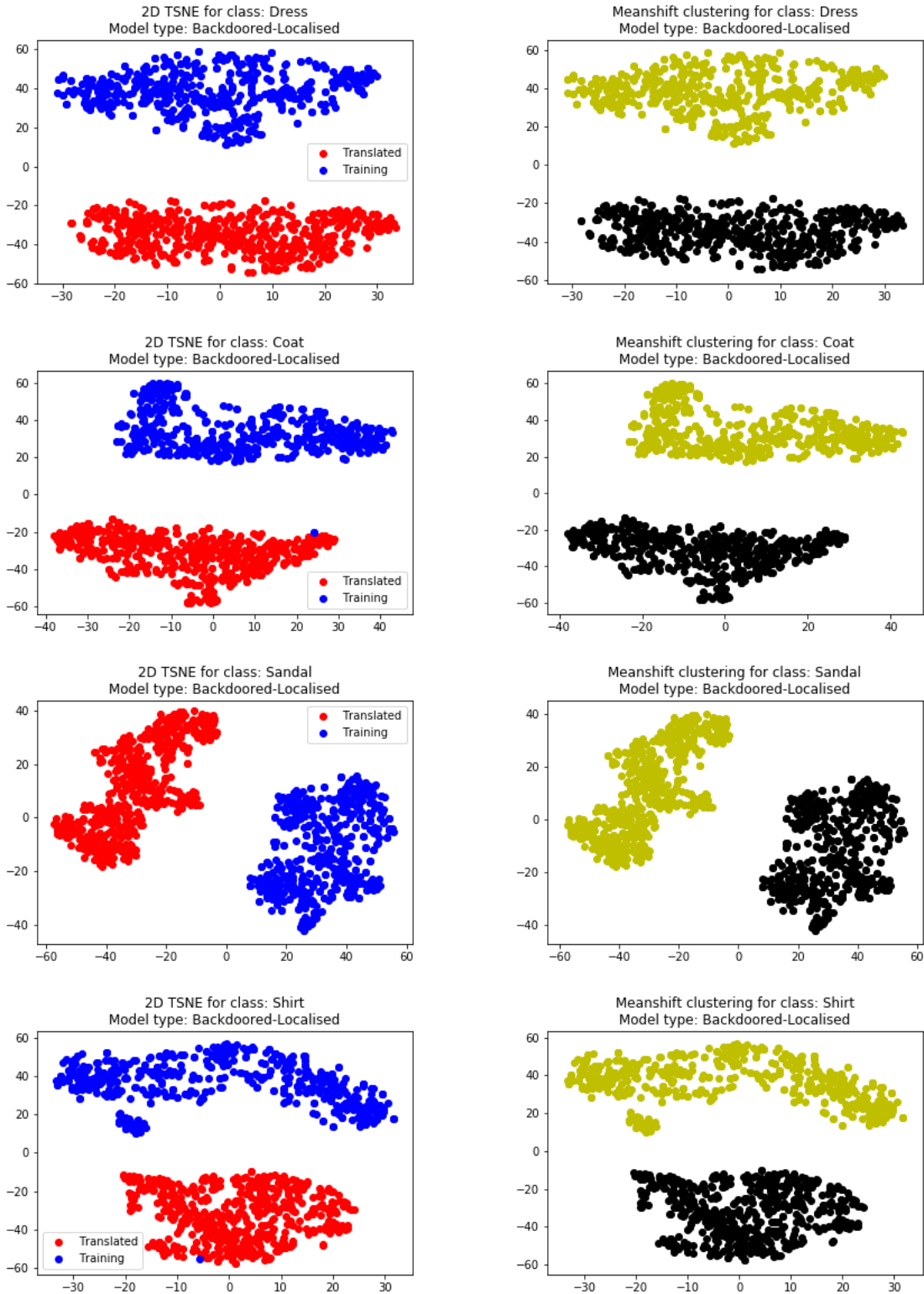


Figure 9. Feature representation clusters for backdoored Fashion-MNIST models (Localised) with target class *Sneaker* (7). Showing class 3 to 6 in this figure. The left column shows the feature representations of the translated and the training images, whereas the right column shows the result of the Mean shift clustering on the corresponding points where different colours represent different classes.

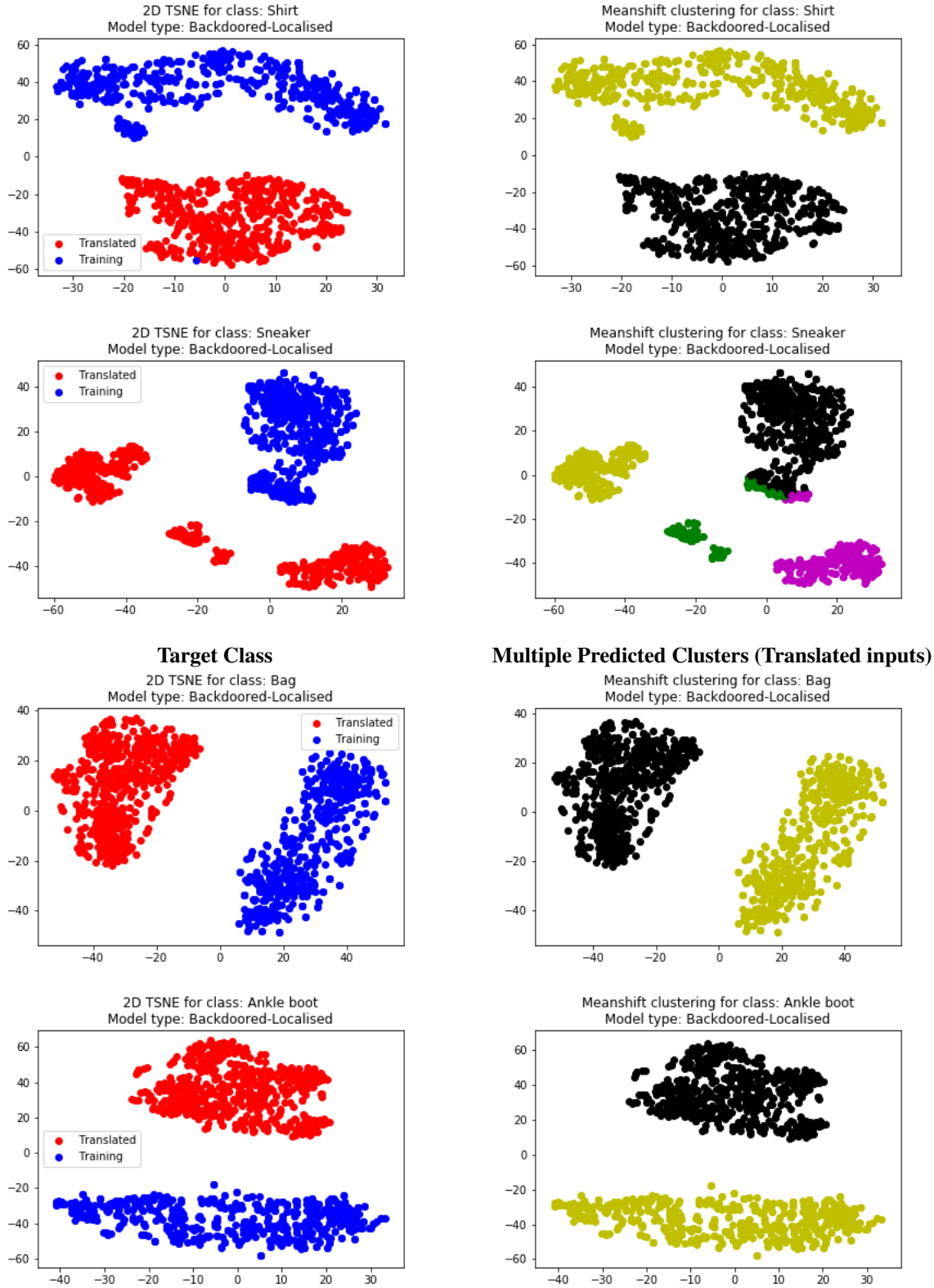


Figure 10. Feature representation clusters for backdoored Fashion-MNIST models (Localised) with target class *Sneaker* (7). Showing class 6 to 9 in this figure. The left column shows the feature representations of the translated and the training images, whereas the right column shows the result of the Mean shift clustering on the corresponding points where different colours represent different classes.

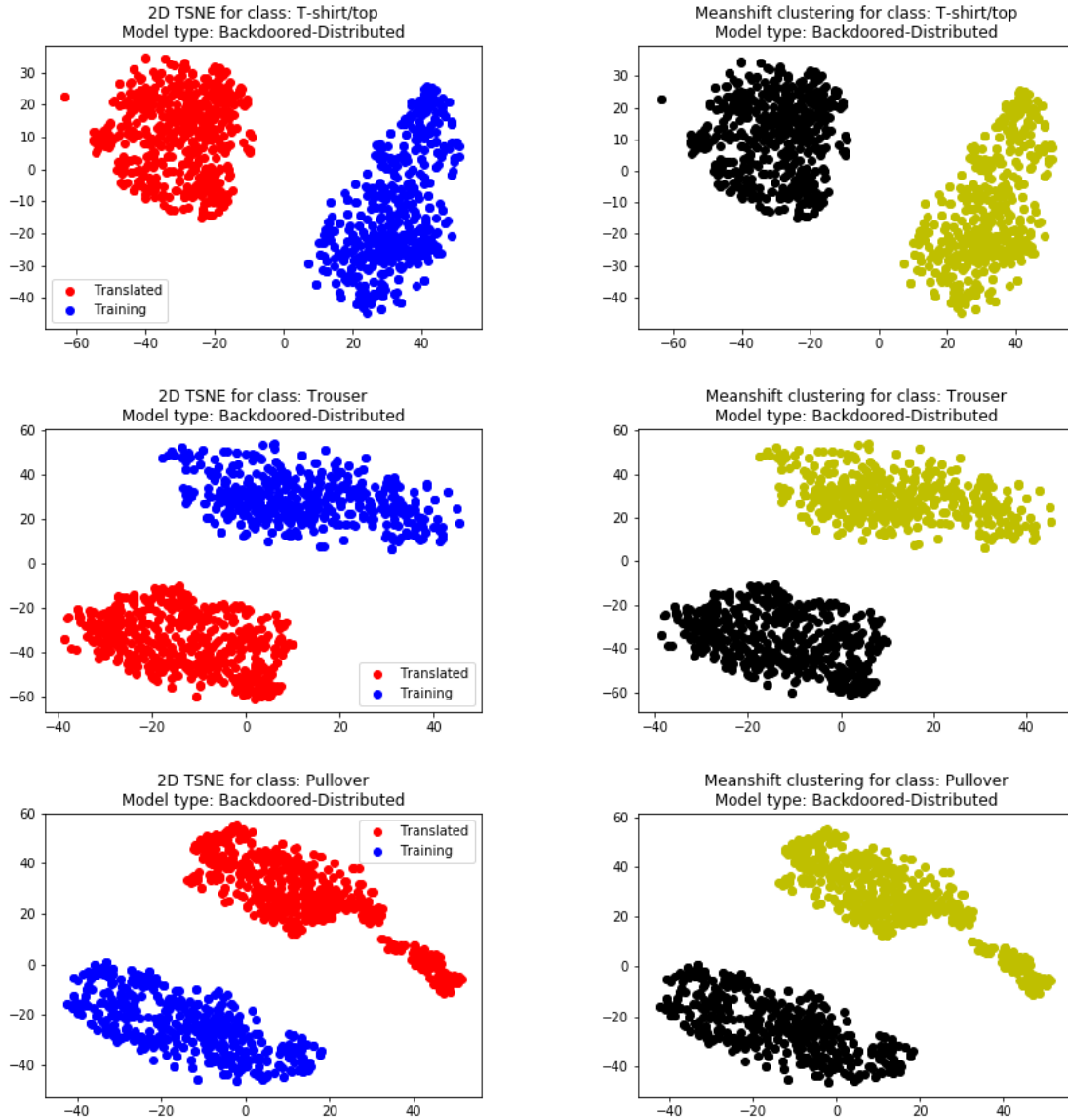


Figure 11. Feature representation clusters for backdoored Fashion-MNIST models (Distributed) with target class *Sneaker* (7). Showing class 0 to 2 in this figure. The left column shows the feature representations of the translated and the training images, whereas the right column shows the result of the Mean shift clustering on the corresponding points where different colours represent different classes.

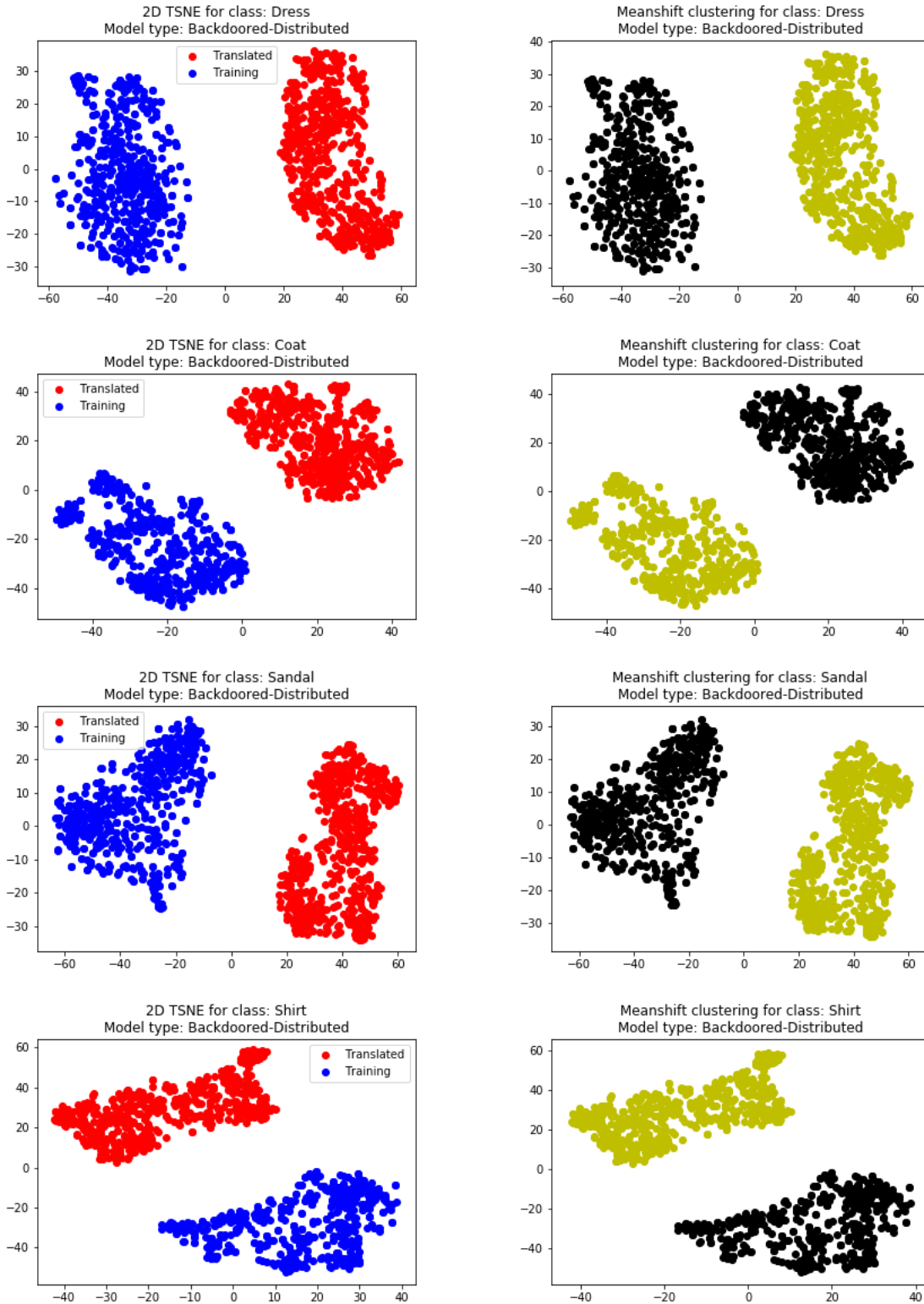


Figure 12. Feature representation clusters for backdoored Fashion-MNIST models (Distributed) with target class *Sneaker* (7). Showing class 3 to 6 in this figure. The left column shows the feature representations of the translated and the training images, whereas the right column shows the result of the Mean shift clustering on the corresponding points where different colours represent different classes.

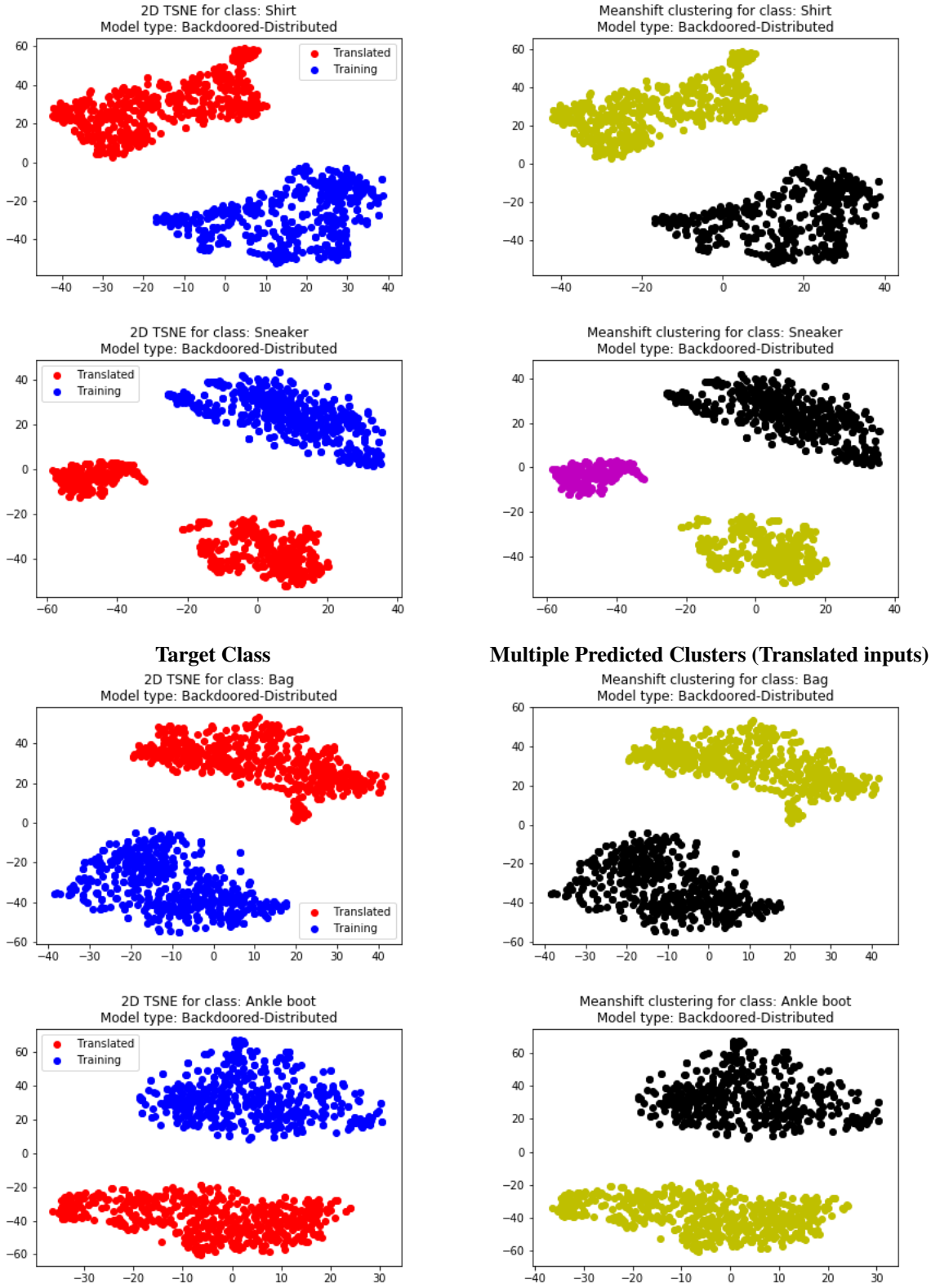


Figure 13. Feature representation clusters for backdoored Fashion-MNIST models (Distributed) with target class *Sneaker* (7). Showing class 6 to 9 in this figure. The left column shows the feature representations of the translated and the training images, whereas the right column shows the result of the Mean shift clustering on the corresponding points.

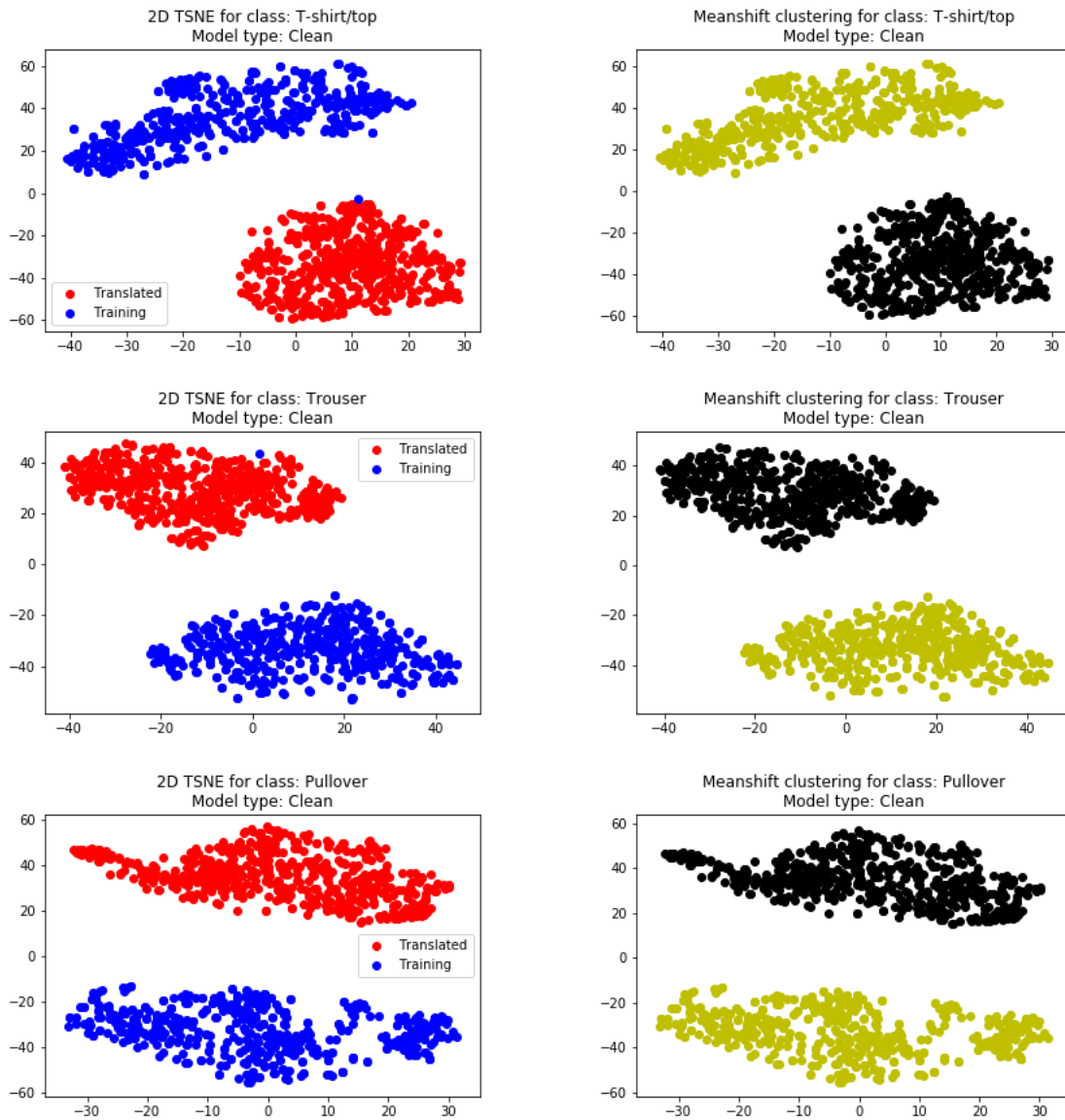


Figure 14. Feature representation clusters for backdoored Fashion-MNIST models (Clean) with target class *Sneaker* (7). Showing class 0 to 2 in this figure. The left column shows the feature representations of the translated and the training images, whereas the right column shows the result of the Mean shift clustering on the corresponding points where different colours represent different classes.

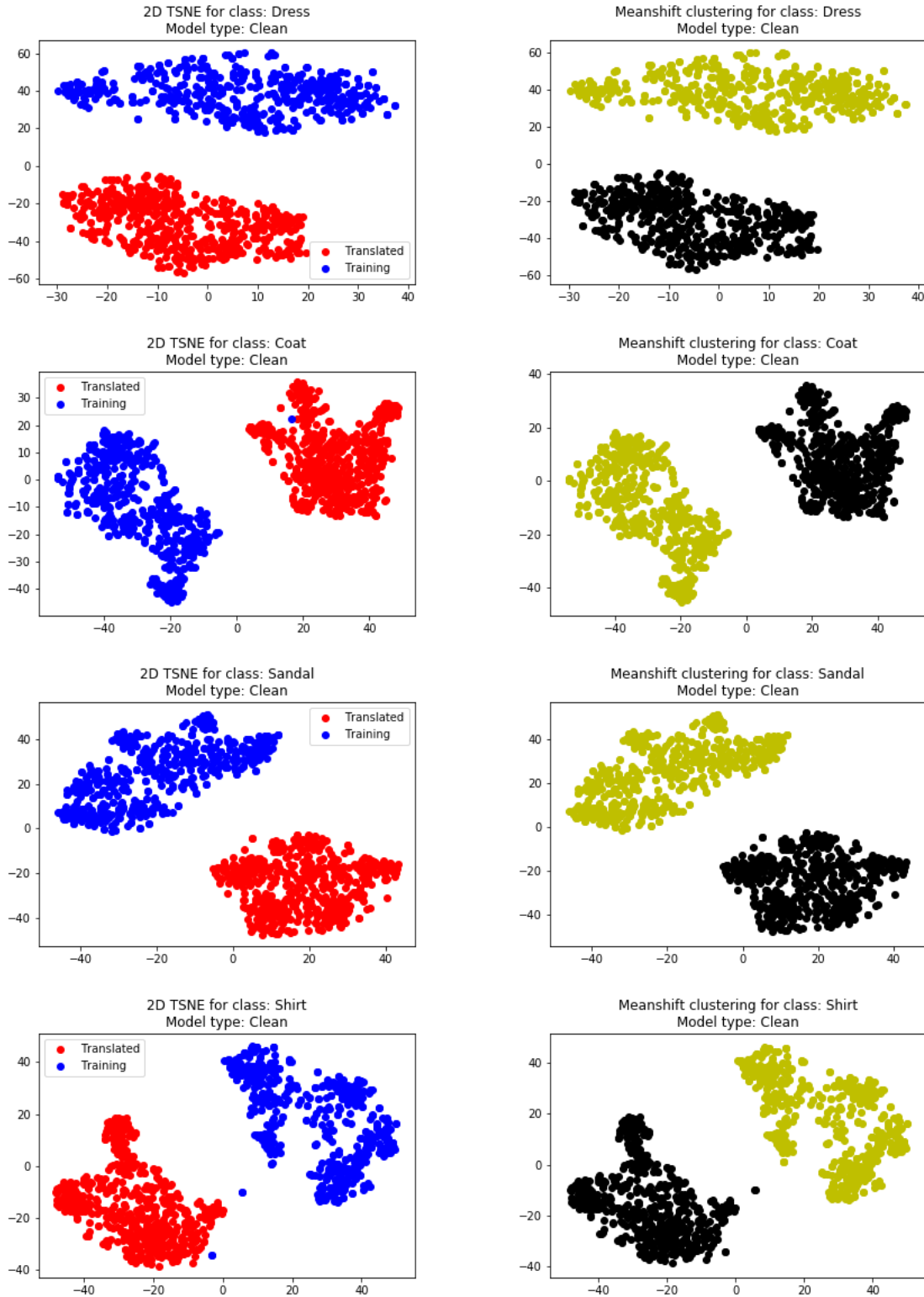


Figure 15. Feature representation clusters for backdoored Fashion-MNIST models (Clean) with target class *Sneaker* (7). Showing class 3 to 6 in this figure. The left column shows the feature representations of the translated and the training images, whereas the right column shows the result of the Mean shift clustering on the corresponding points where different colours represent different classes.

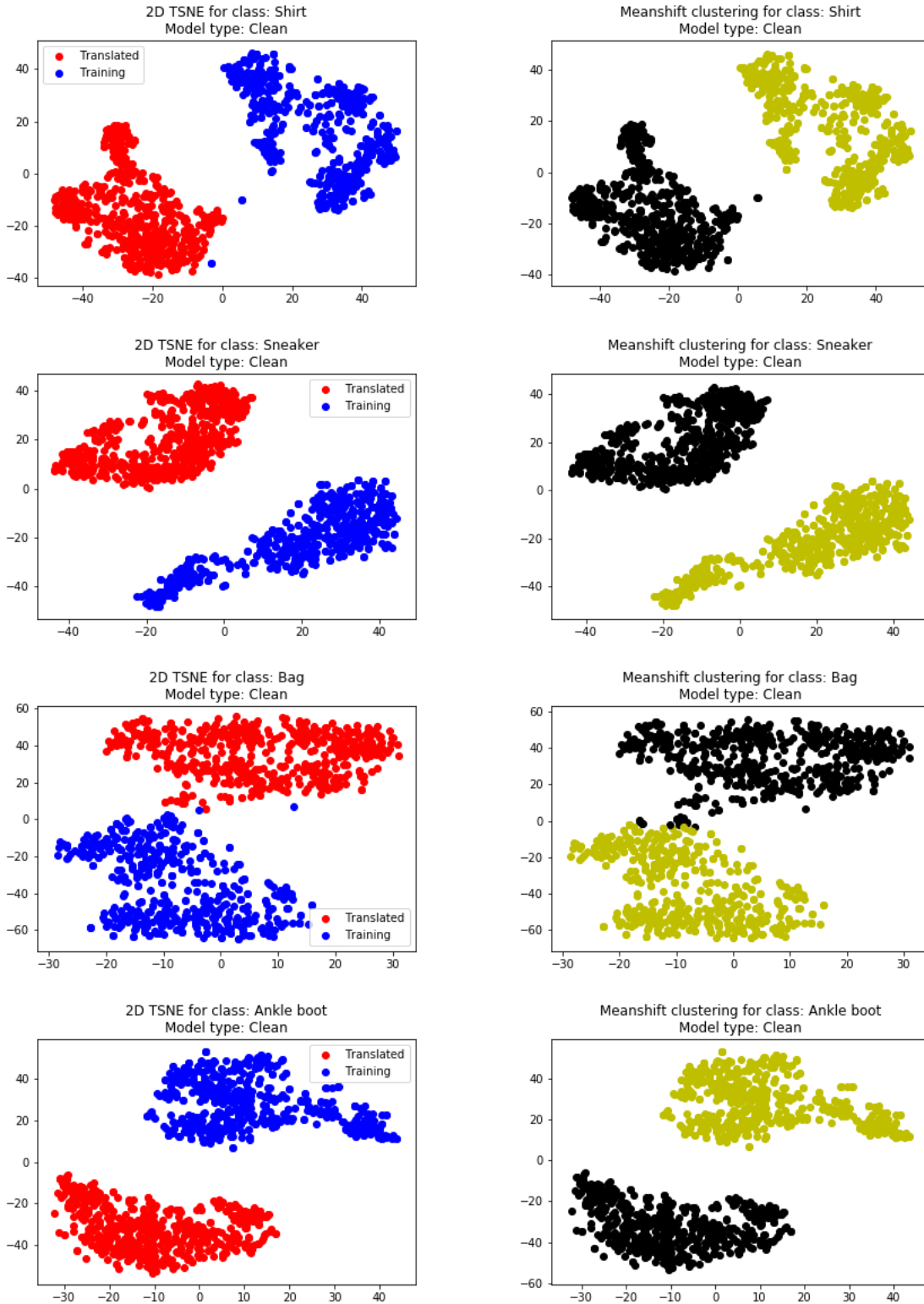


Figure 16. Feature representation clusters for backdoored Fashion-MNIST models (Clean) with target class *Sneaker* (7). Showing class 6 to 9 in this figure. The left column shows the feature representations of the translated and the training images, whereas the right column shows the result of the Mean shift clustering on the corresponding points where different colours represent different classes.

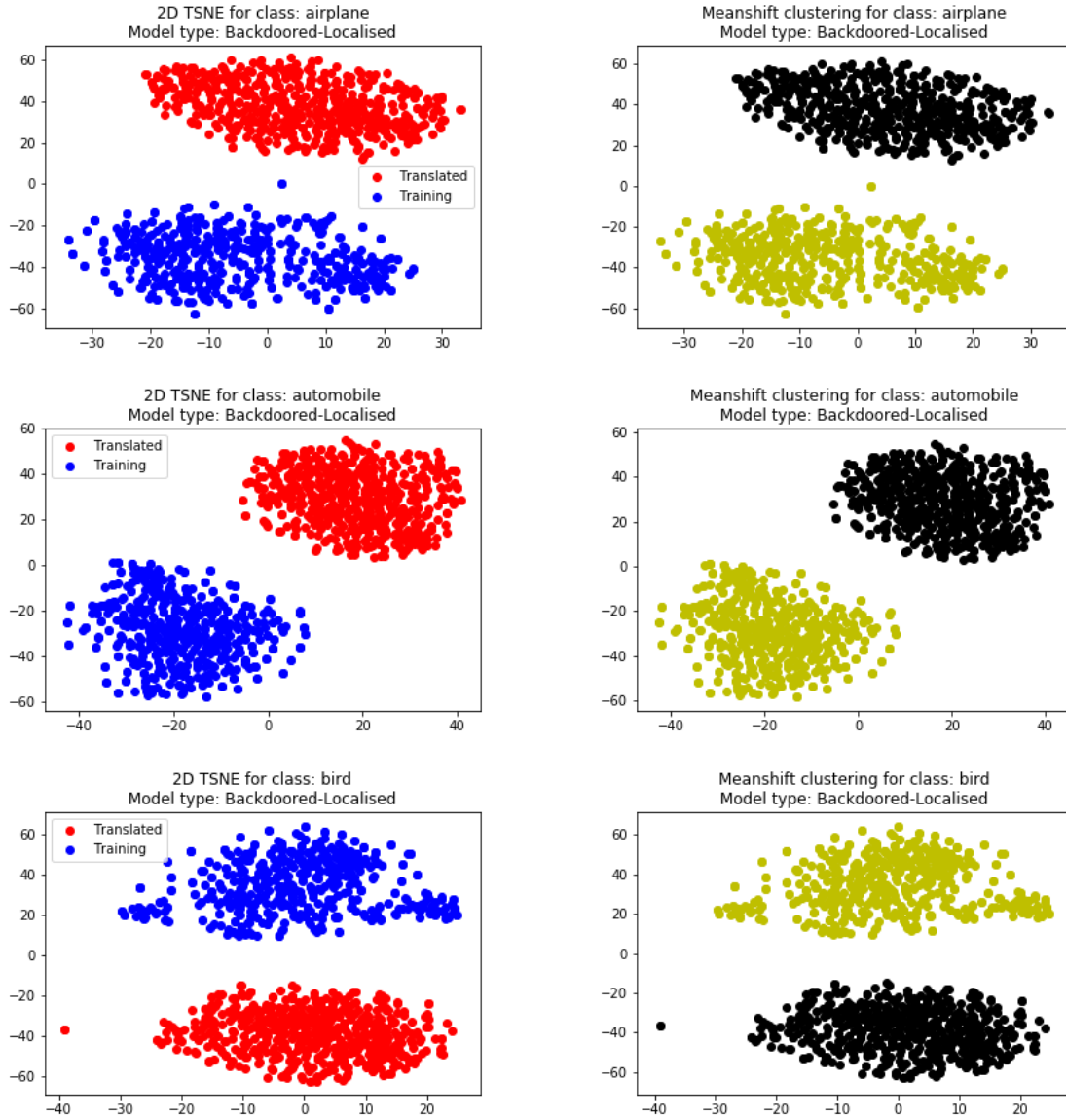


Figure 17. Feature representation clusters for backdoored CIFAR models (Localised) with target class *Horse* (7). Showing class 0 to 2 in this figure. The left column shows the feature representations of the translated and the training images, whereas the right column shows the result of the Mean shift clustering on the corresponding points where different colours represent different classes.

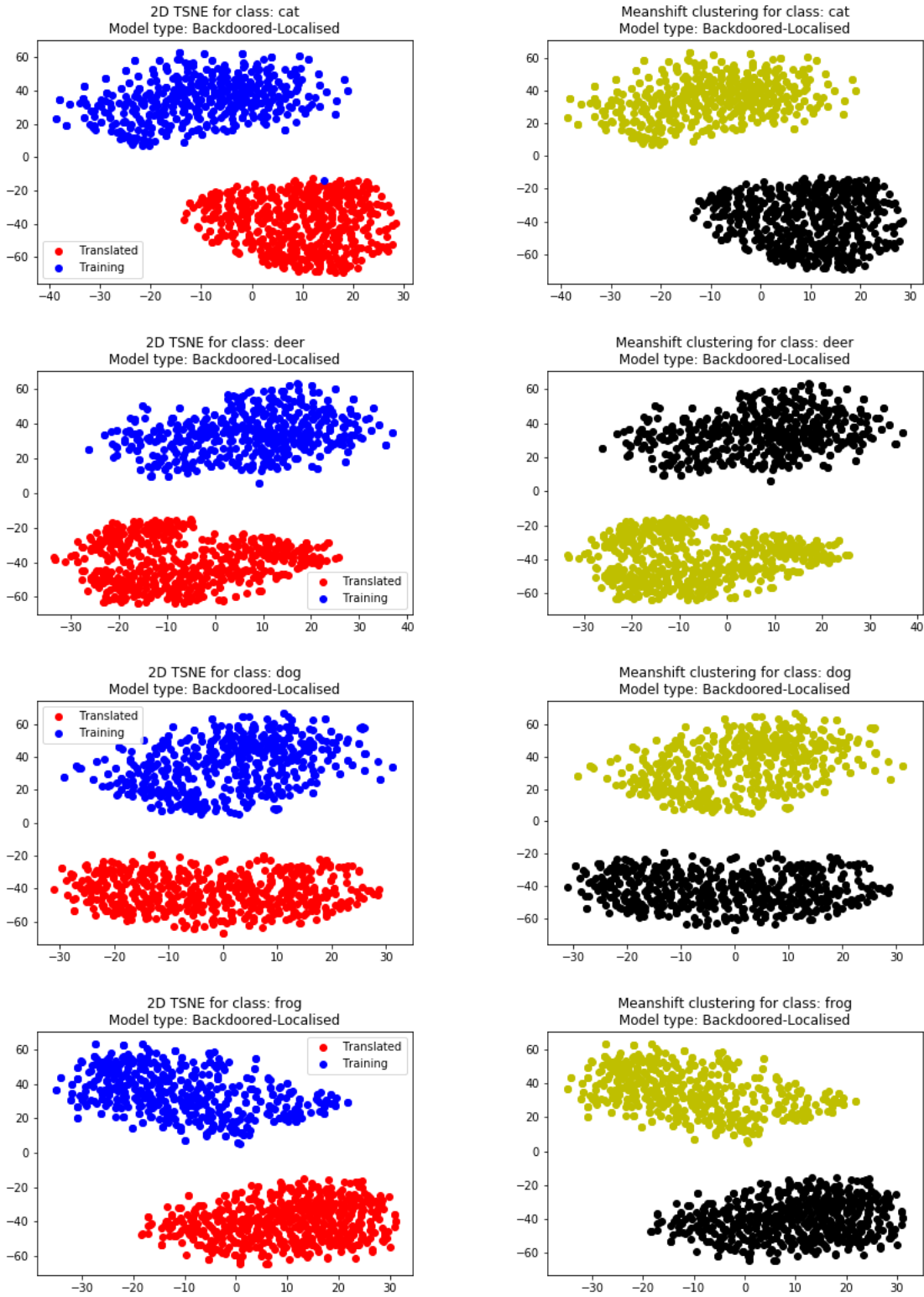


Figure 18. Feature representation clusters for backdoored CIFAR models (Localised) with target class *Horse* (7). Showing class 3 to 6 in this figure. The left column shows the feature representations of the translated and the training images, whereas the right column shows the result of the Mean shift clustering on the corresponding points where different colours represent different classes.

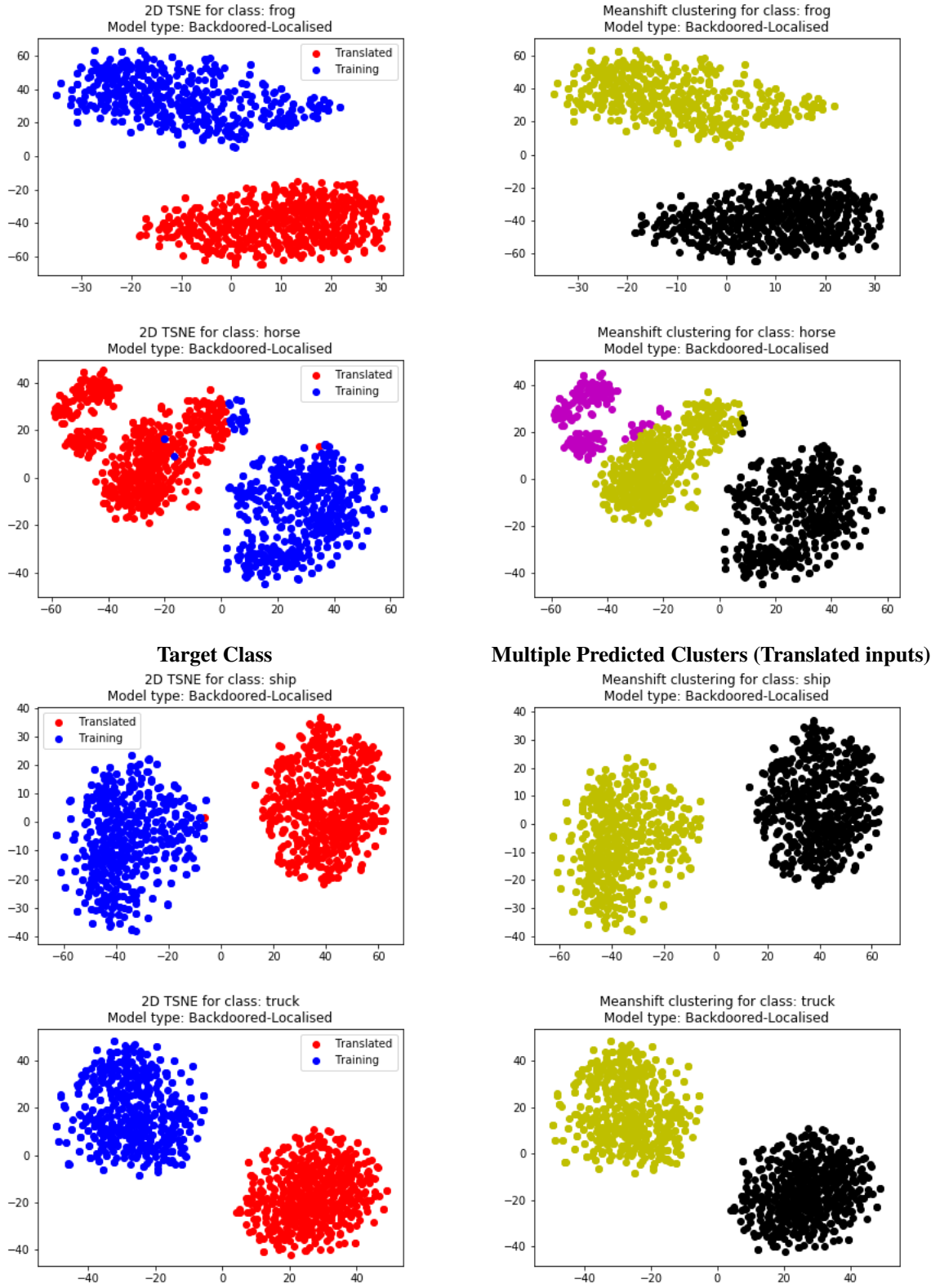


Figure 19. Feature representation clusters for backdoored CIFAR models (Localised) with target class *Horse* (7). Showing class 6 to 9 in this figure. The left column shows the feature representations of the translated and the training images, whereas the right column shows the result of the Mean shift clustering on the corresponding points where different colours represent different classes.

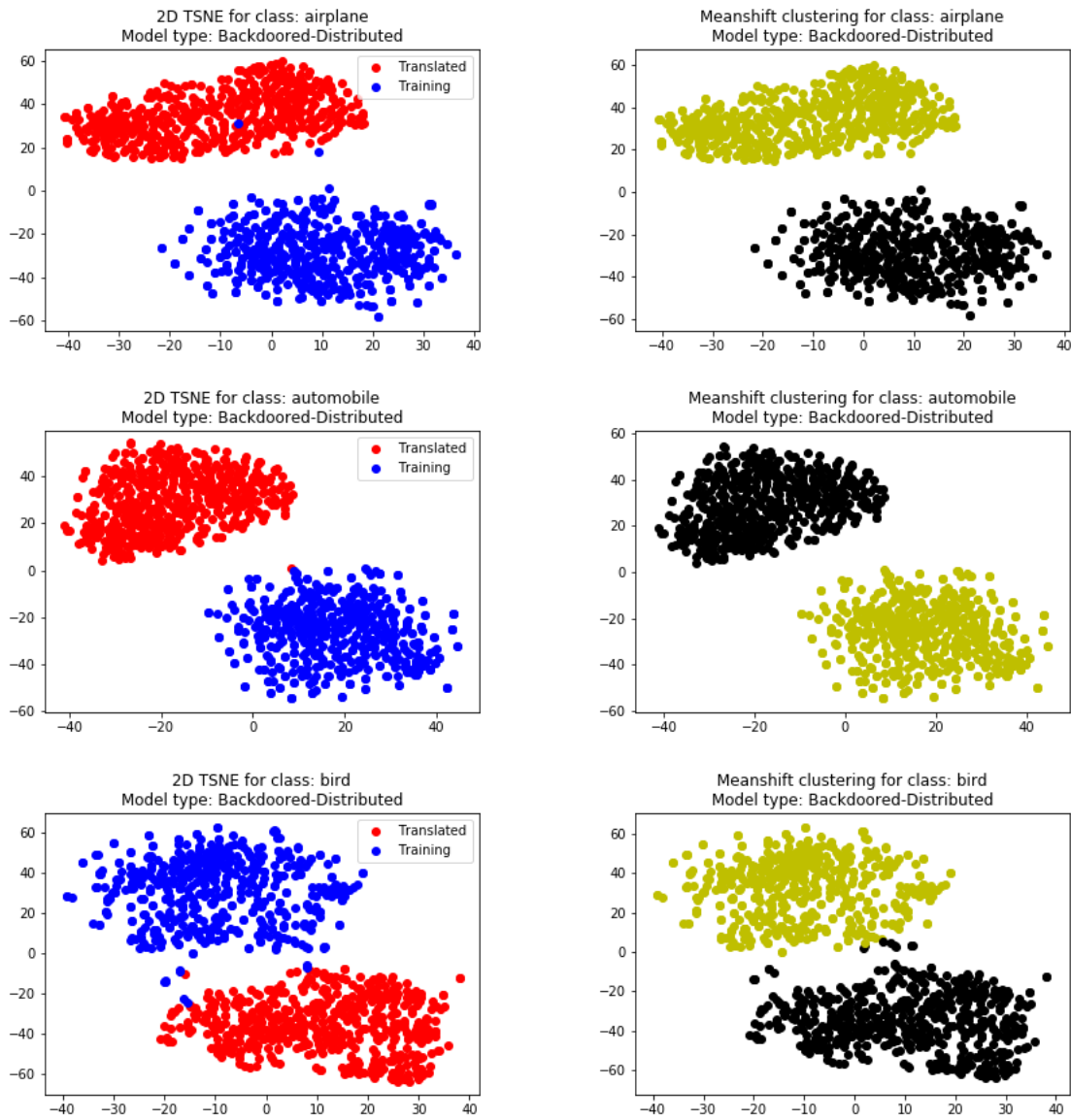


Figure 20. Feature representation clusters for backdoored CIFAR models (Distributed) with target class *Horse* (7). Showing class 0 to 2 in this figure. The left column shows the feature representations of the translated and the training images, whereas the right column shows the result of the Mean shift clustering on the corresponding points where different colours represent different classes.

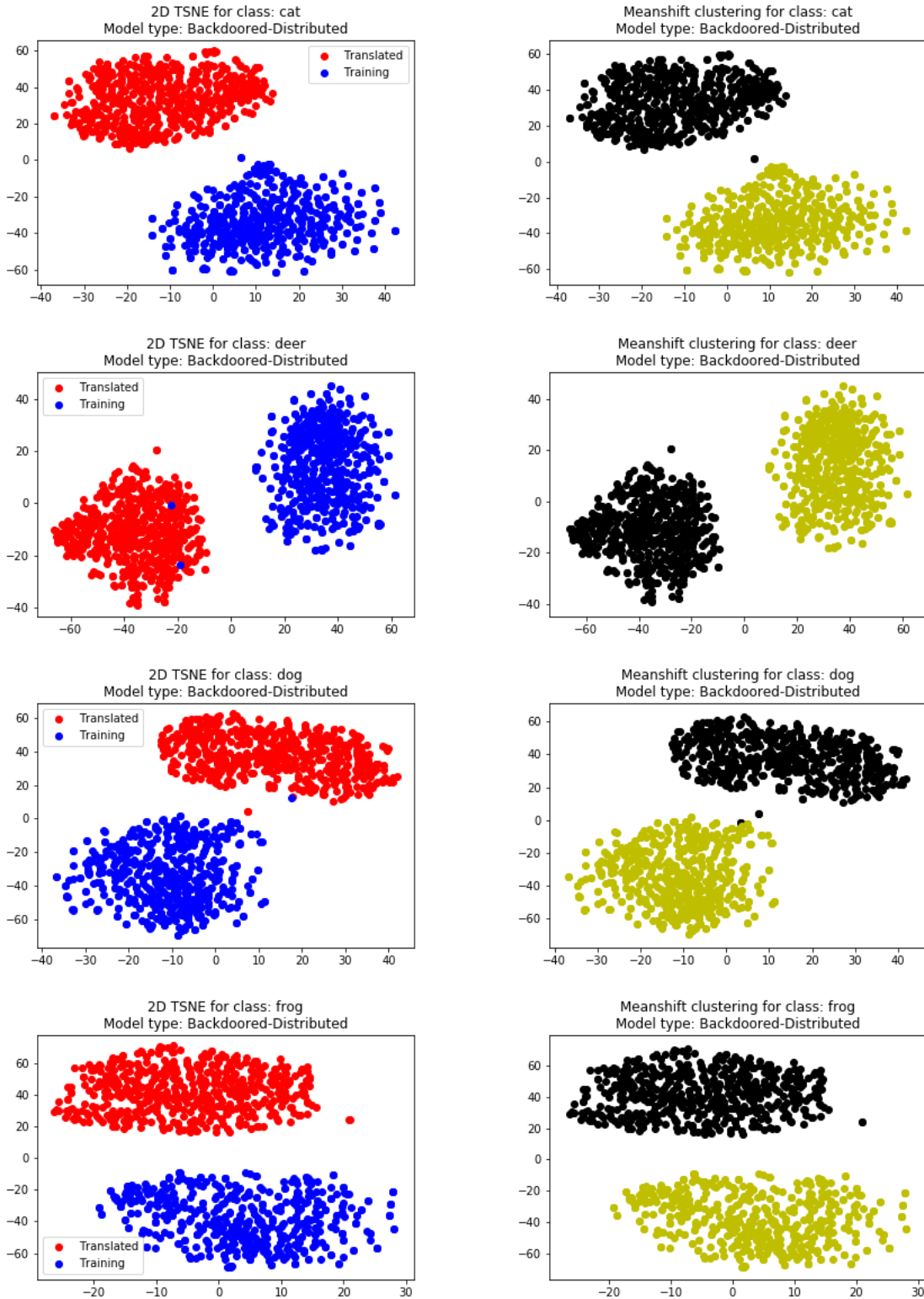


Figure 21. Feature representation clusters for backdoored CIFAR models (Distributed) with target class *Horse* (7). Showing class 3 to 6 in this figure. The left column shows the feature representations of the translated and the training images, whereas the right column shows the result of the Mean shift clustering on the corresponding points where different colours represent different classes.

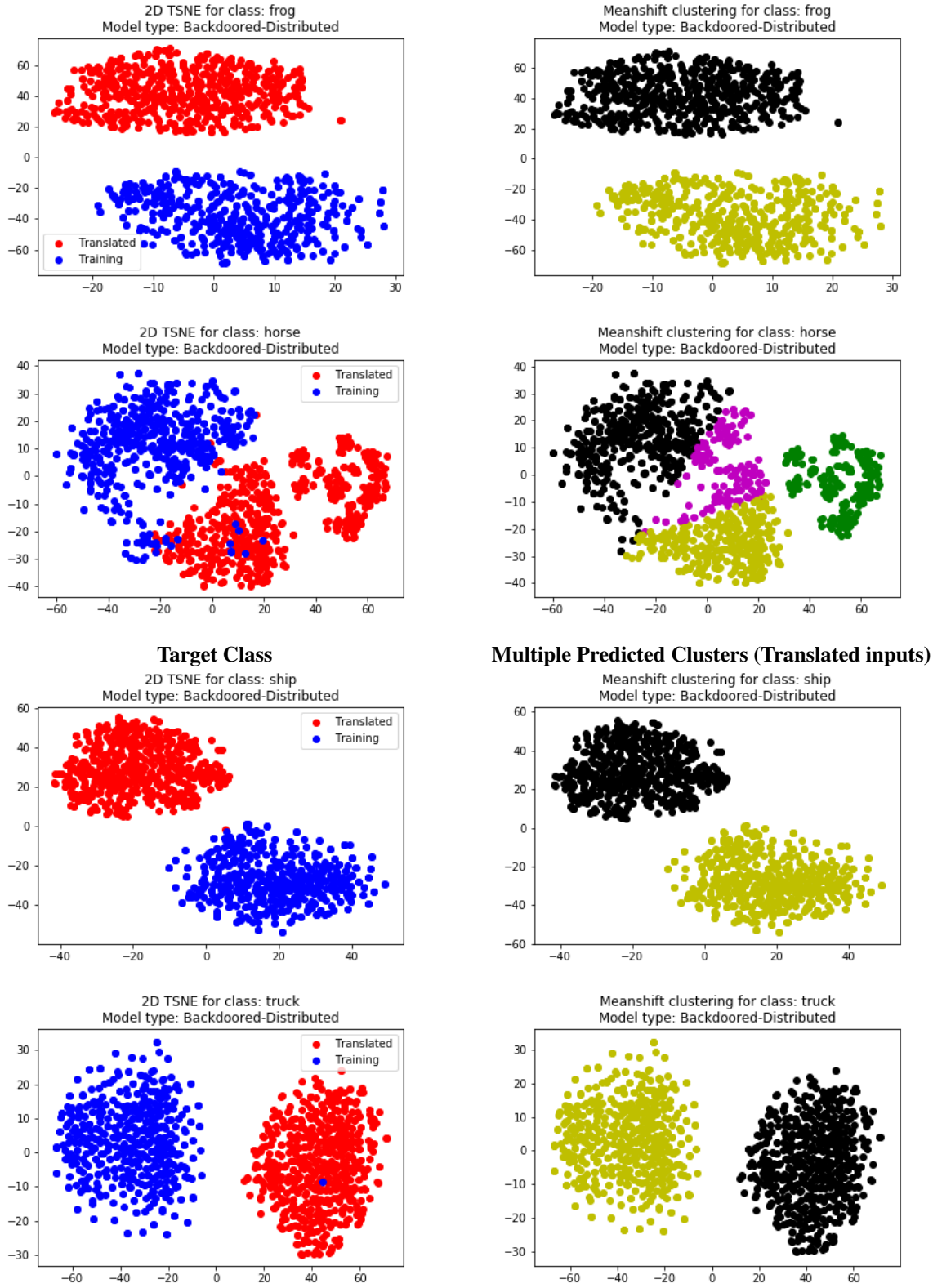


Figure 22. Feature representation clusters for backdoored CIFAR models (Distributed) with target class *Horse* (7). Showing class 6 to 9 in this figure. The left column shows the feature representations of the translated and the training images, whereas the right column shows the result of the Mean shift clustering on the corresponding points.

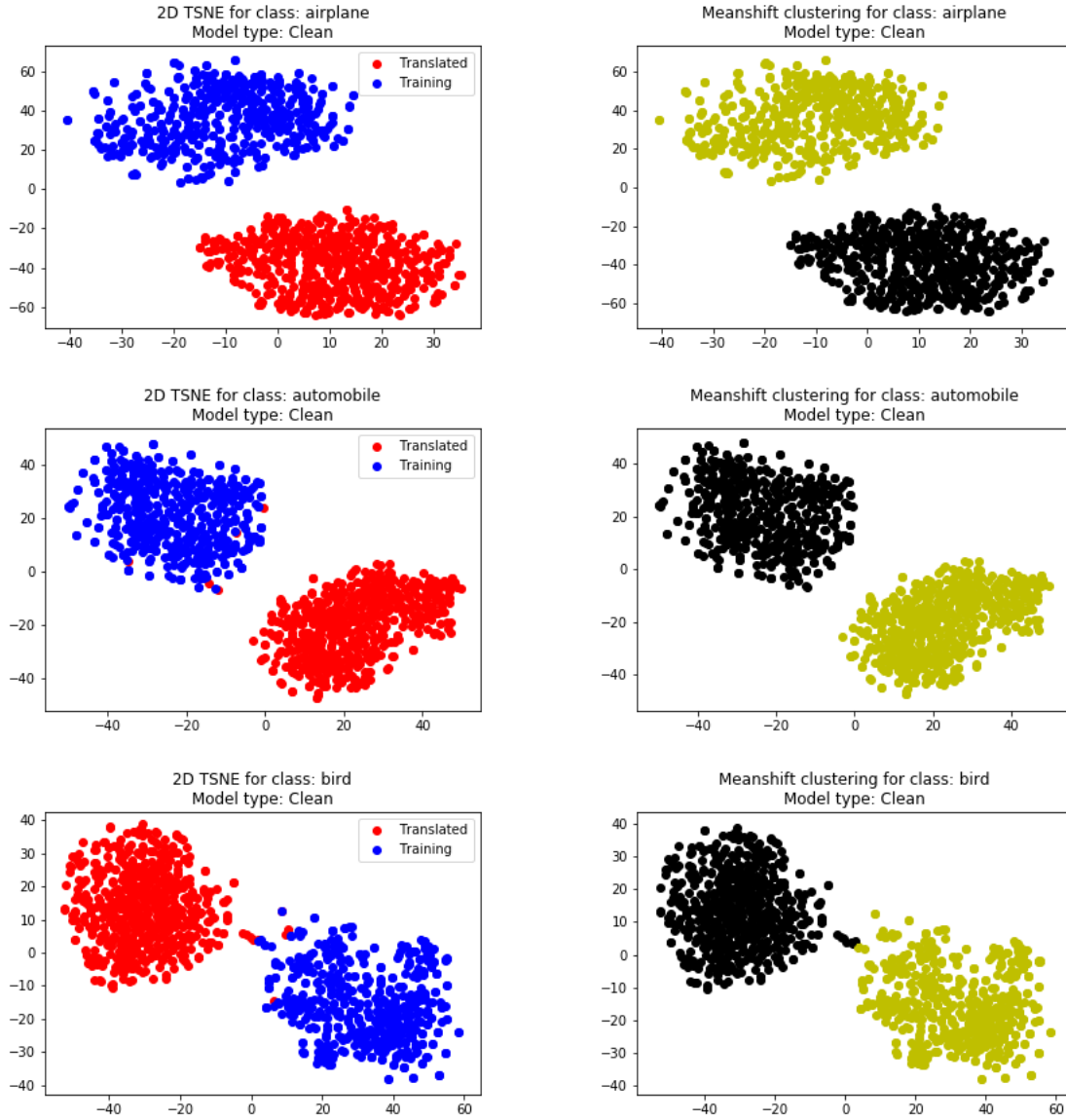


Figure 23. Feature representation clusters for backdoored CIFAR models (Clean) with target class *Horse* (7). Showing class 0 to 2 in this figure. The left column shows the feature representations of the translated and the training images, whereas the right column shows the result of the Mean shift clustering on the corresponding points where different colours represent different classes.

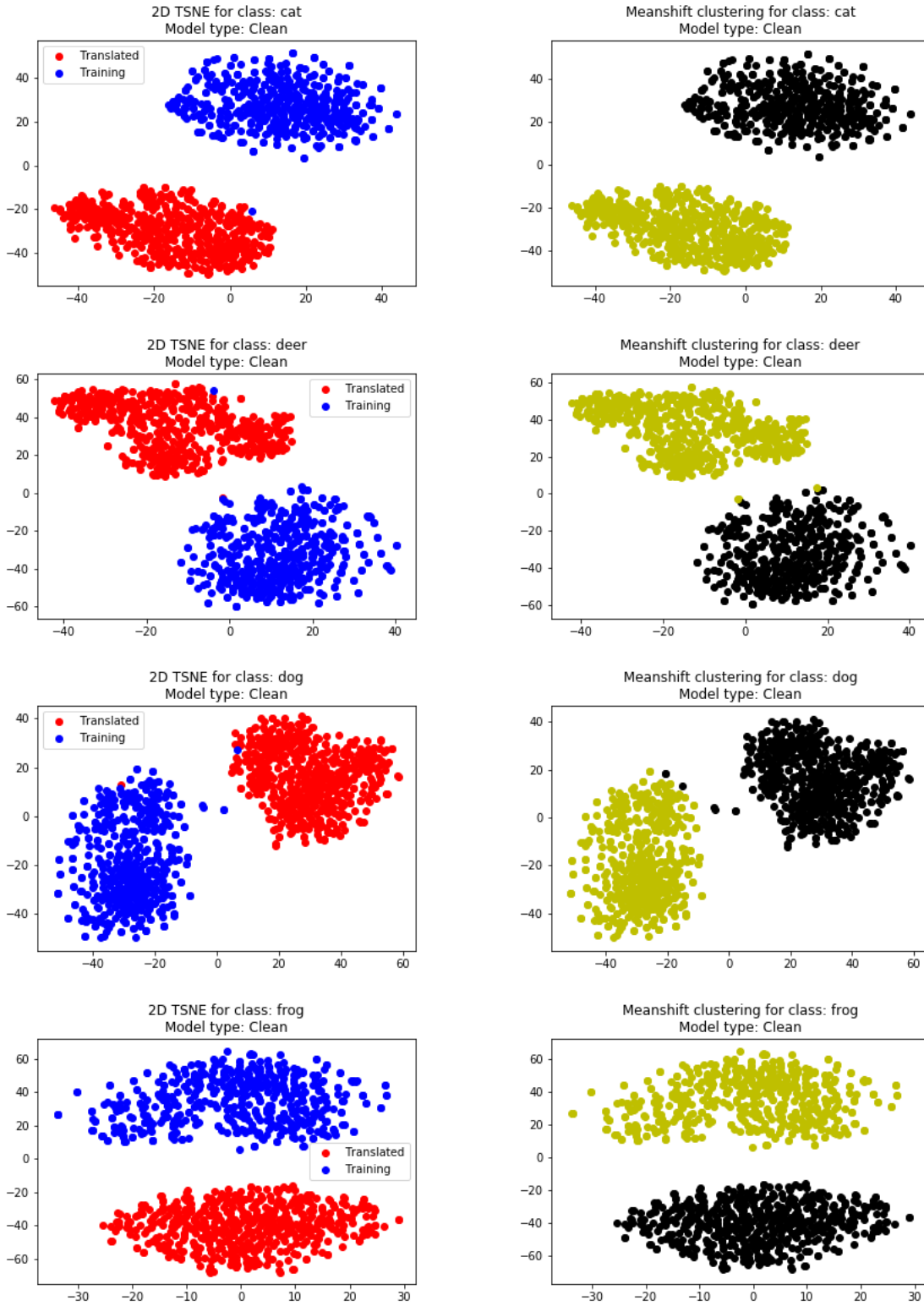


Figure 24. Feature representation clusters for backdoored CIFAR models (Clean) with target class *Horse* (7). Showing class 3 to 6 in this figure. The left column shows the feature representations of the translated and the training images, whereas the right column shows the result of the Mean shift clustering on the corresponding points where different colours represent different classes.

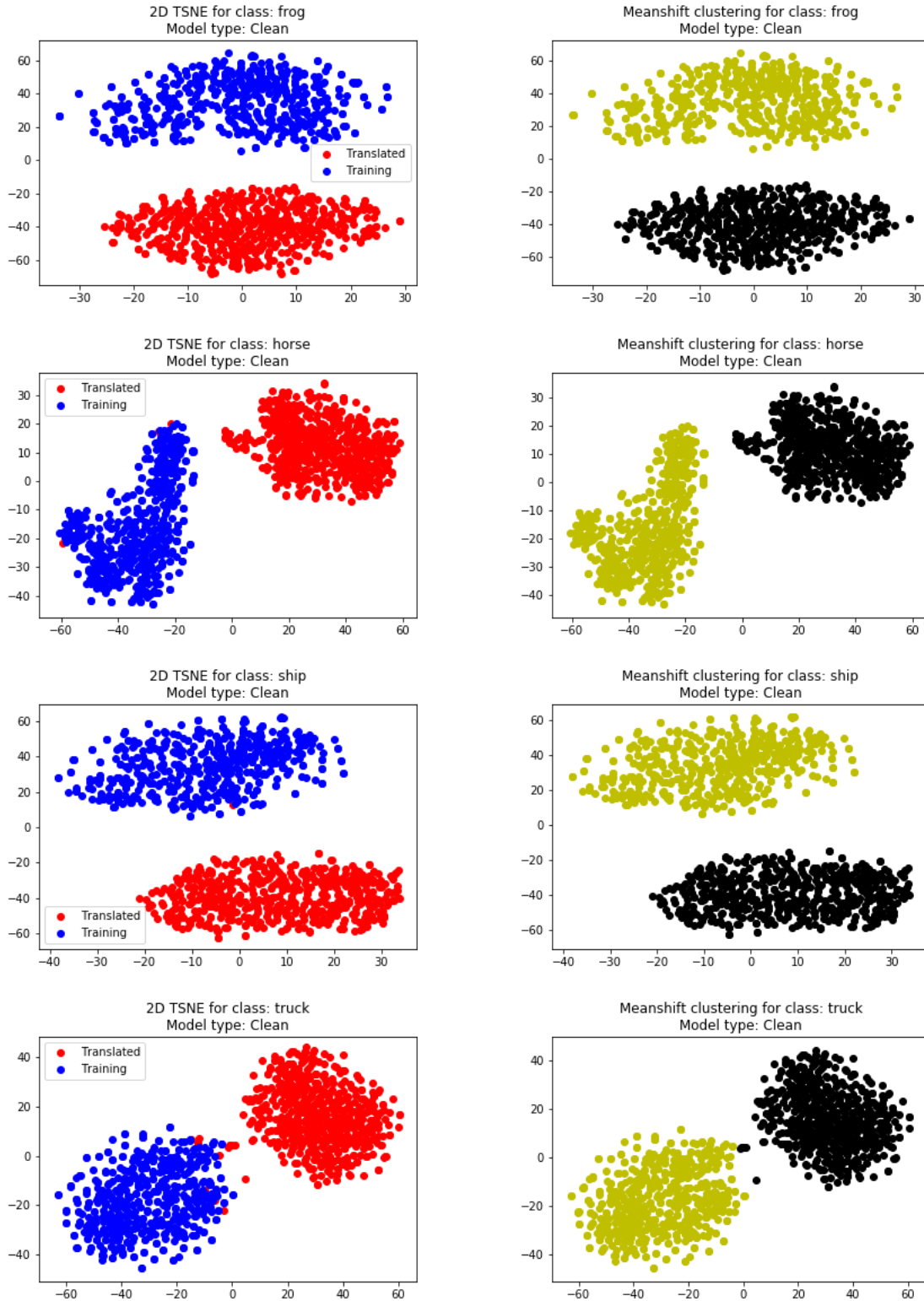


Figure 25. Feature representation clusters for backdoored CIFAR models (Clean) with target class *Horse* (7). Showing class 6 to 9 in this figure. The left column shows the feature representations of the translated and the training images, whereas the right column shows the result of the Mean shift clustering on the corresponding points where different colours represent different classes.

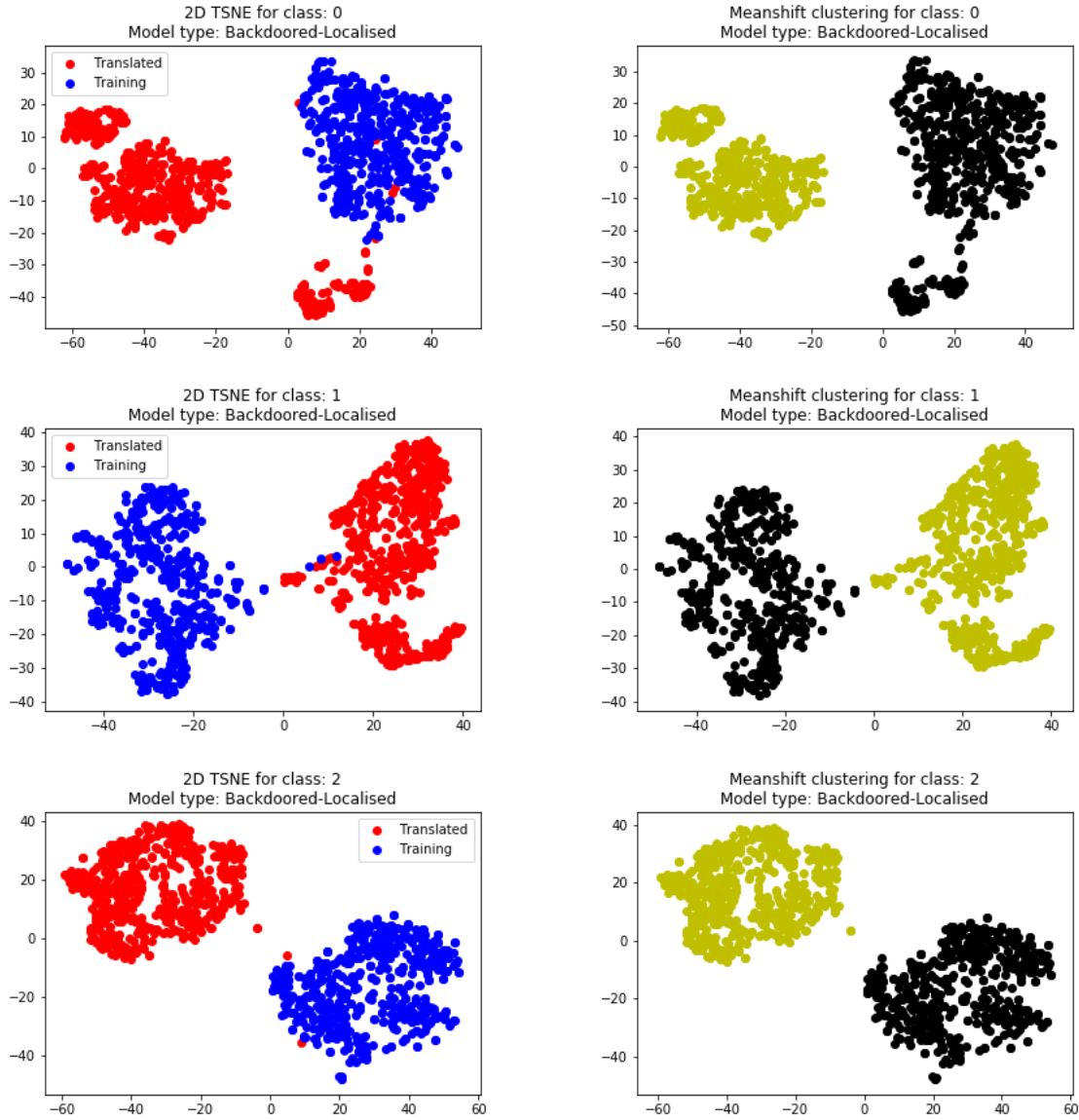


Figure 26. Feature representation clusters for backdoored MNIST models (Localised) with target class 7. Showing class 0 to 2 in this figure. The left column shows the feature representations of the translated and the training images, whereas the right column shows the result of the Mean shift clustering on the corresponding points where different colours represent different classes.

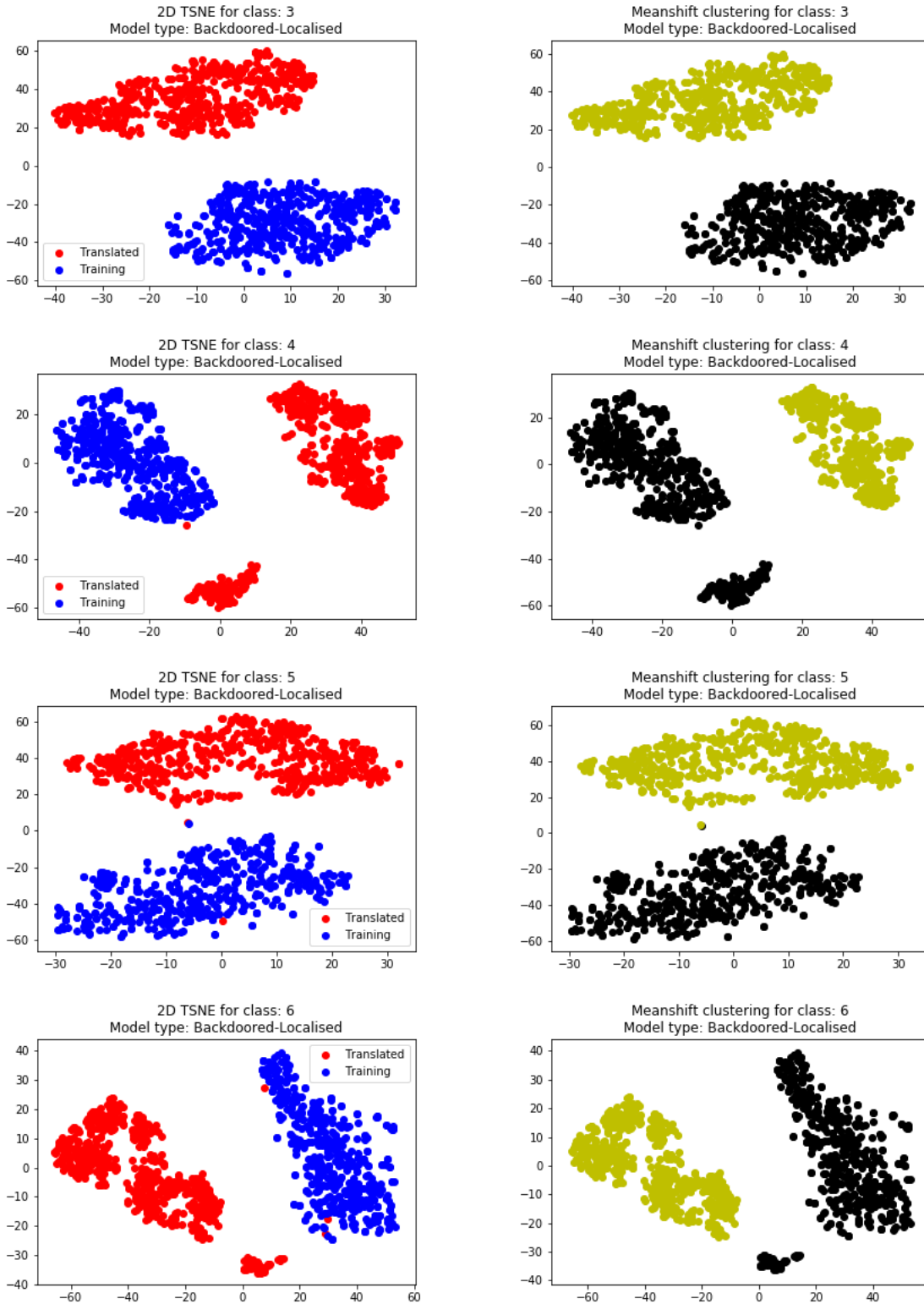


Figure 27. Feature representation clusters for backdoored MNIST models (Localised) with target class 7. Showing class 3 to 6 in this figure. The left column shows the feature representations of the translated and the training images, whereas the right column shows the result of the Mean shift clustering on the corresponding points where different colours represent different classes.

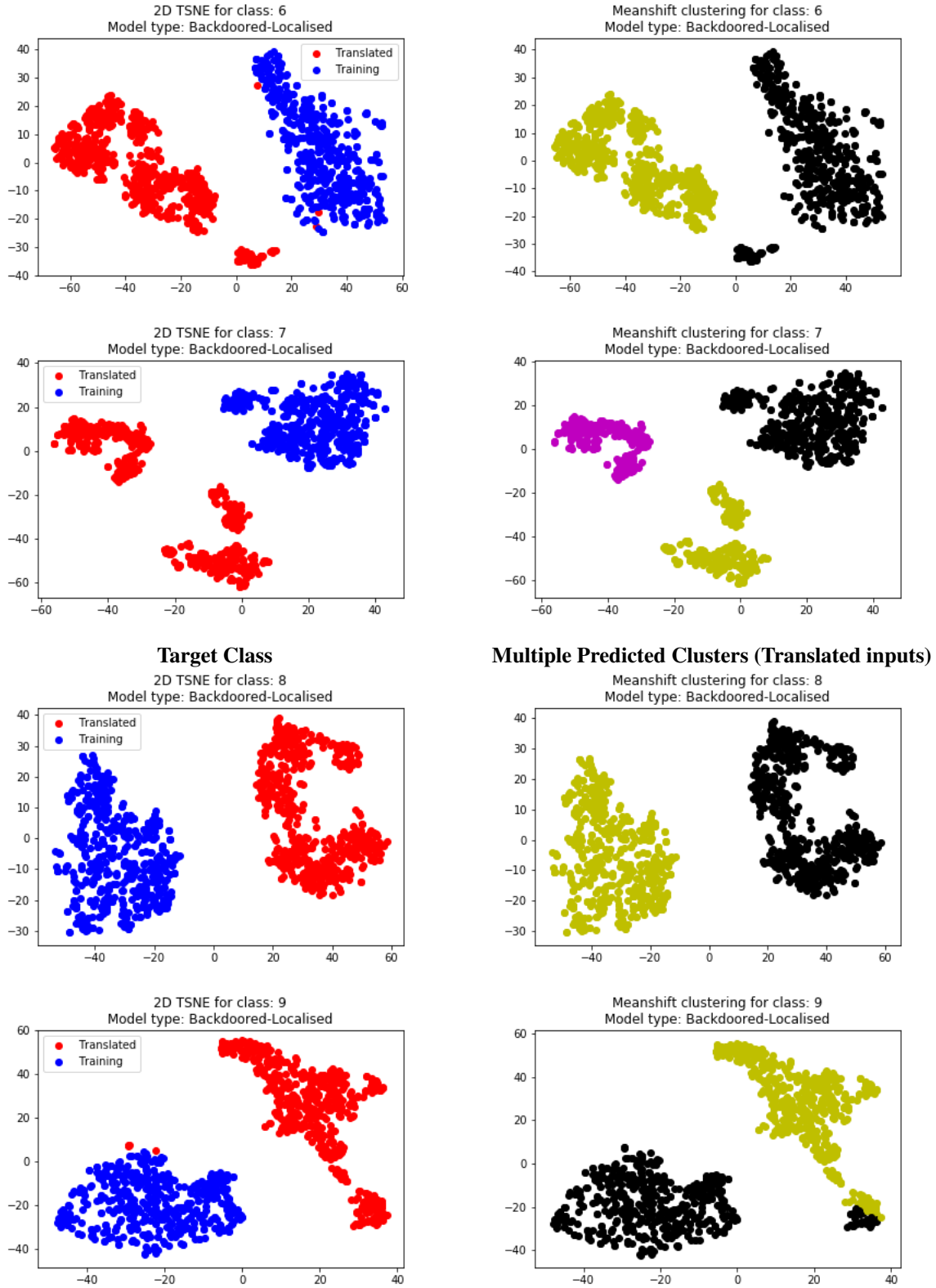


Figure 28. Feature representation clusters for backdoored MNIST models (Localised) with target class 7. Showing class 6 to 9 in this figure. The left column shows the feature representations of the translated and the training images, whereas the right column shows the result of the Mean shift clustering on the corresponding points where different colours represent different classes.

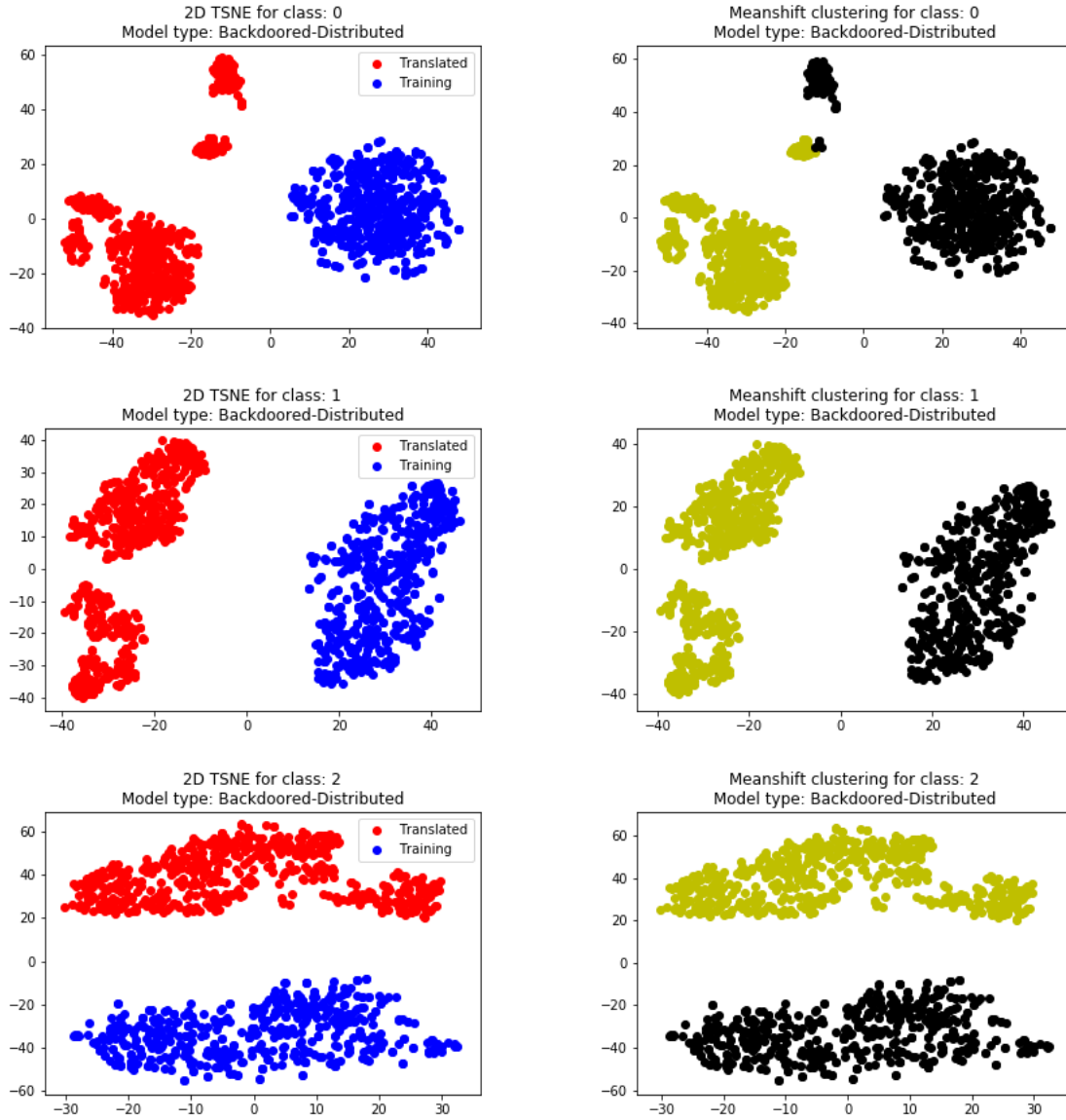


Figure 29. Feature representation clusters for backdoored MNIST models (Distributed) with target class 7. Showing class 0 to 2 in this figure. The left column shows the feature representations of the translated and the training images, whereas the right column shows the result of the Mean shift clustering on the corresponding points where different colours represent different classes.

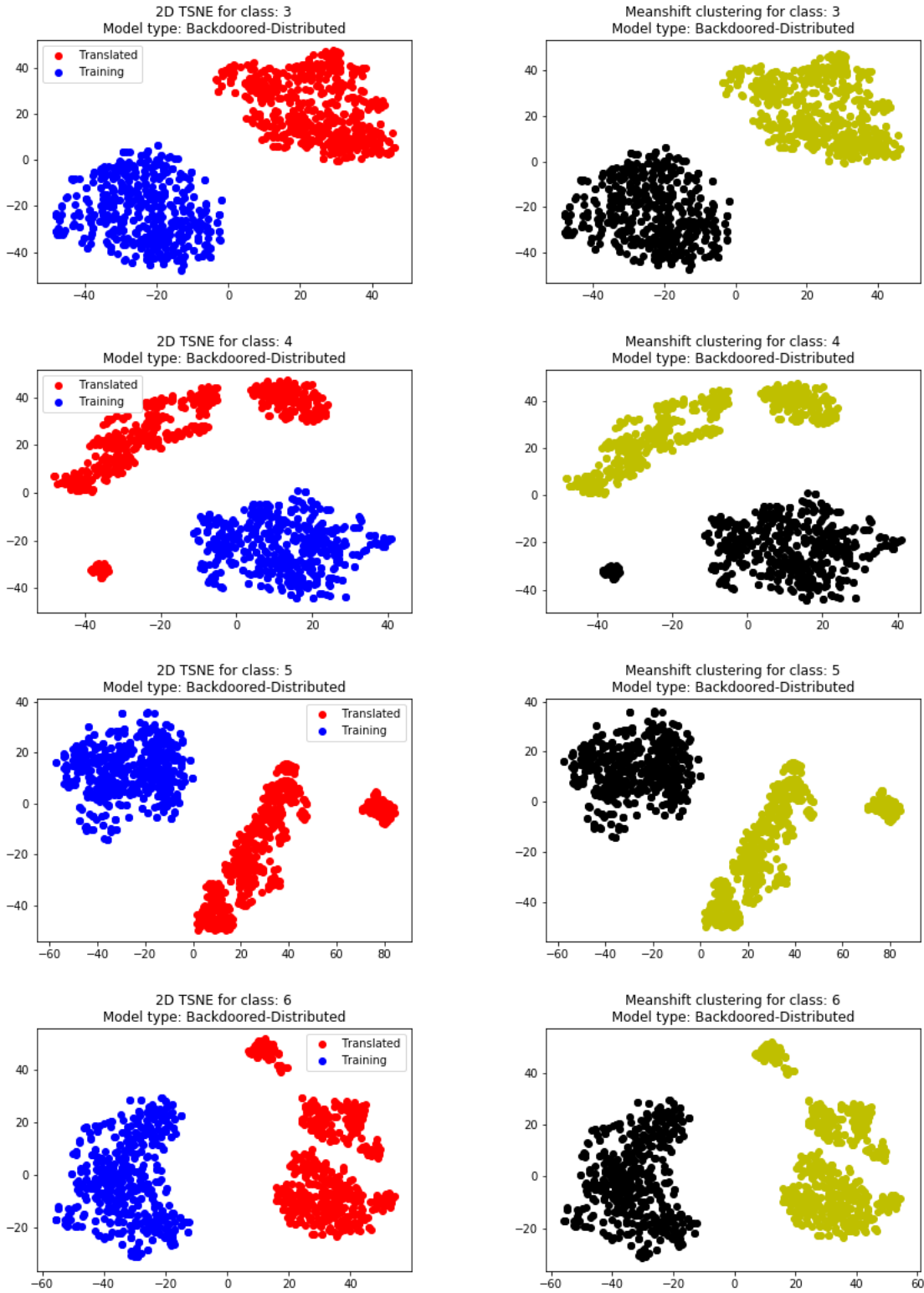


Figure 30. Feature representation clusters for backdoored MNIST models (Distributed) with target class 7. Showing class 3 to 6 in this figure. The left column shows the feature representations of the translated and the training images, whereas the right column shows the result of the Mean shift clustering on the corresponding points where different colours represent different classes.

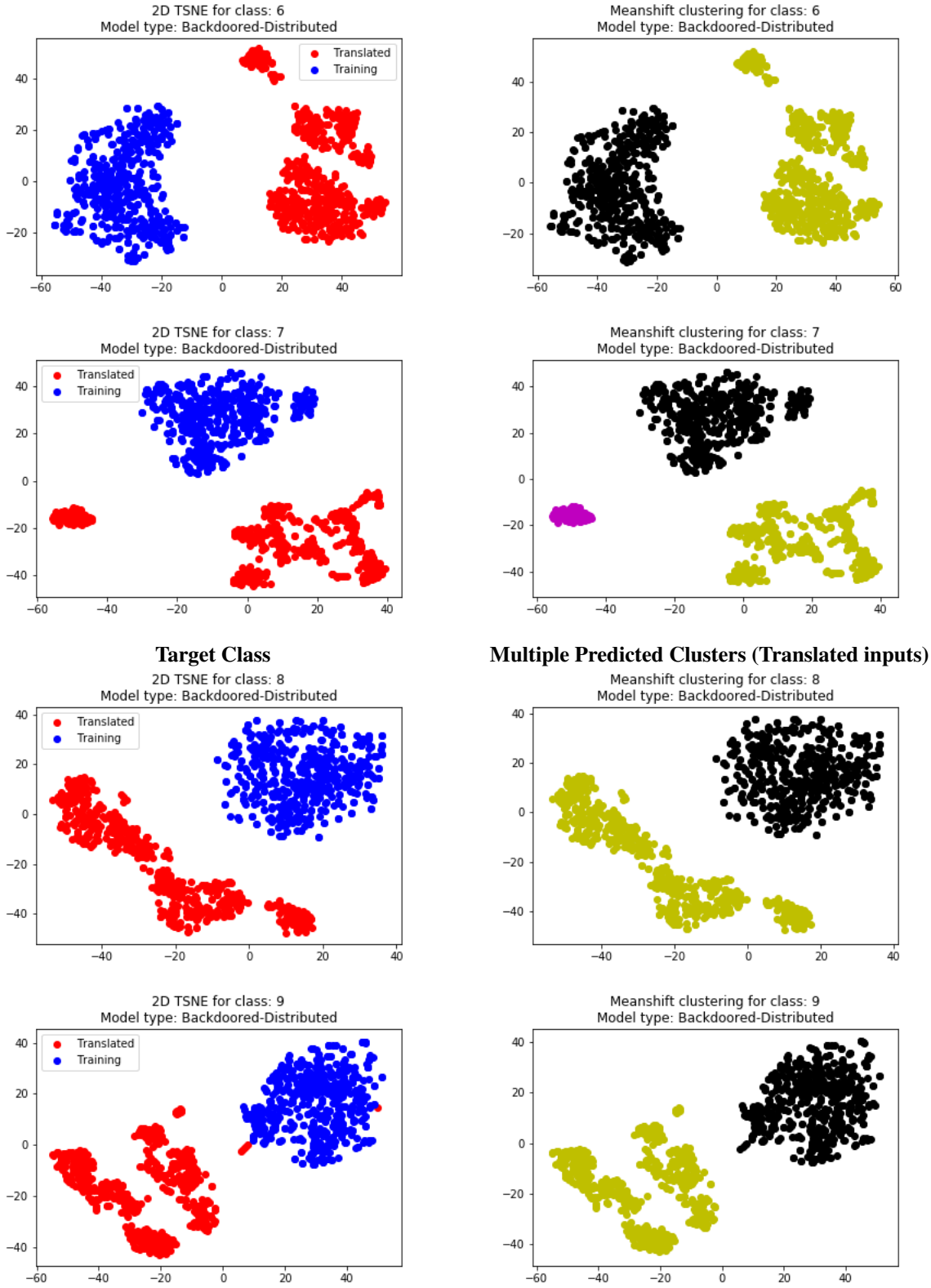


Figure 31. Feature representation clusters for backdoored MNIST models (Distributed) with target class 7. Showing class 6 to 9 in this figure. The left column shows the feature representations of the translated and the training images, whereas the right column shows the result of the Mean shift clustering on the corresponding points.

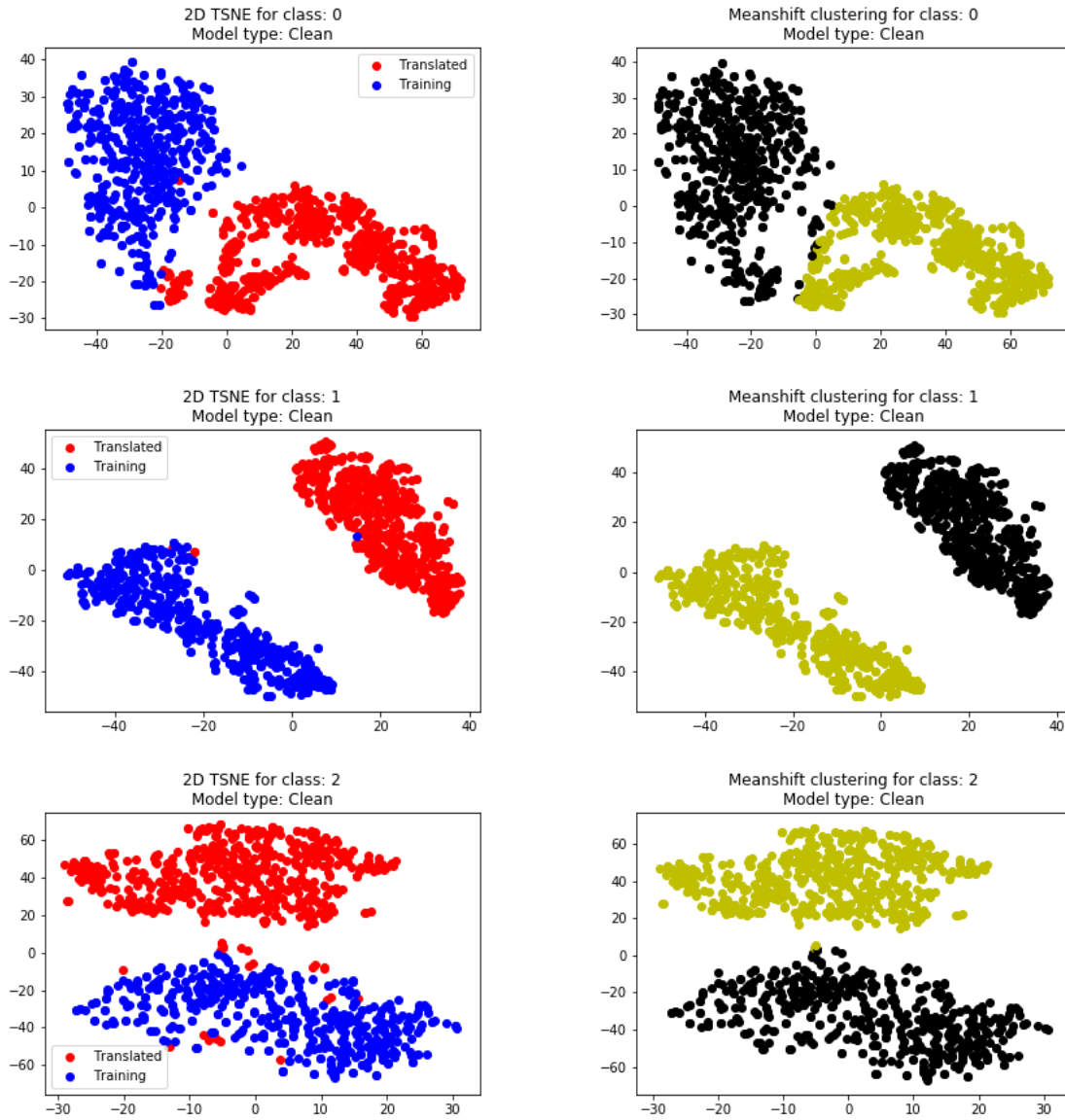


Figure 32. Feature representation clusters for backdoored MNIST models (Clean) with target class 7. Showing class 0 to 2 in this figure. The left column shows the feature representations of the translated and the training images, whereas the right column shows the result of the Mean shift clustering on the corresponding points where different colours represent different classes.

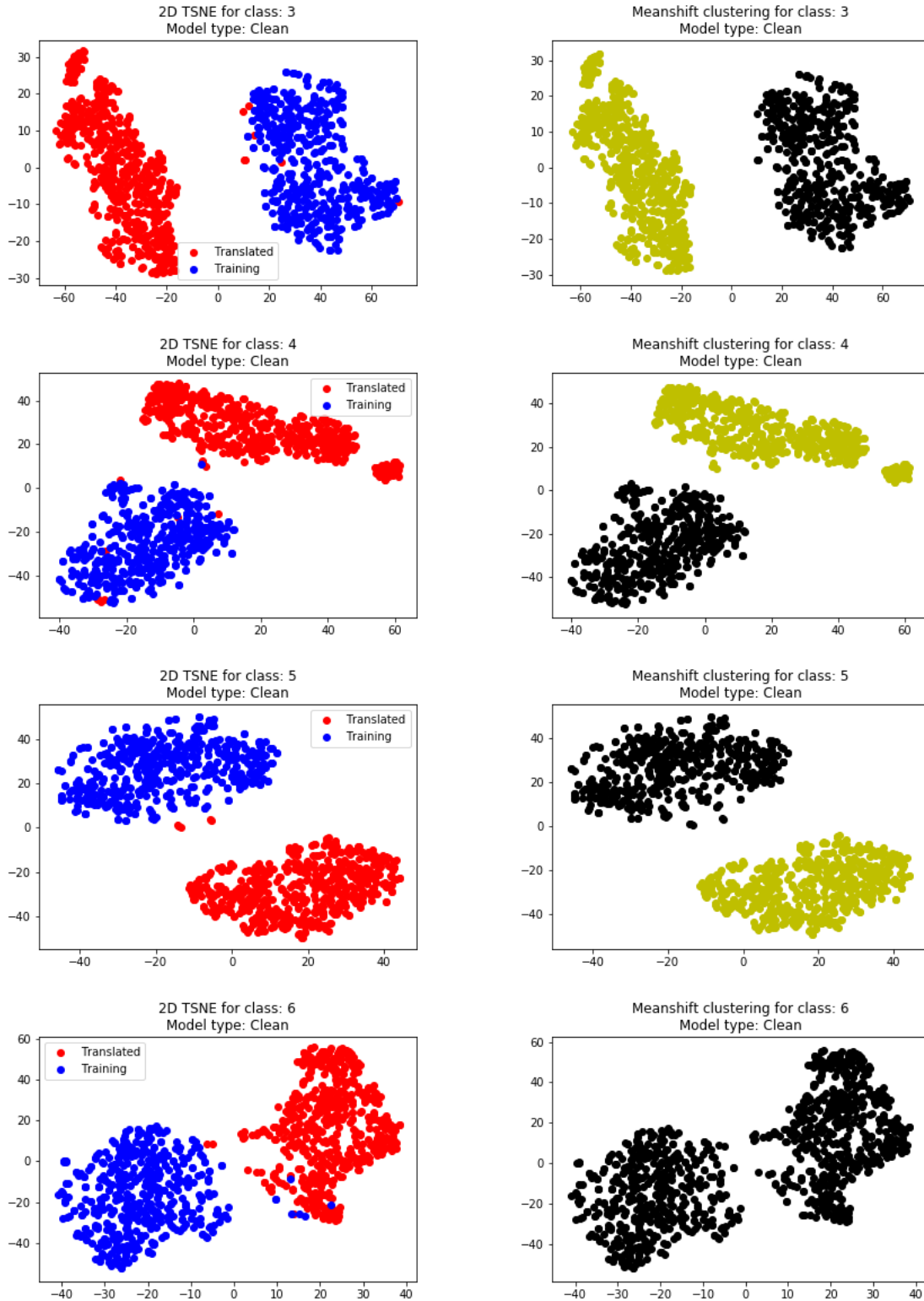


Figure 33. Feature representation clusters for backdoored MNIST models (Clean) with target class 7. Showing class 3 to 6 in this figure. The left column shows the feature representations of the translated and the training images, whereas the right column shows the result of the Mean shift clustering on the corresponding points where different colours represent different classes.

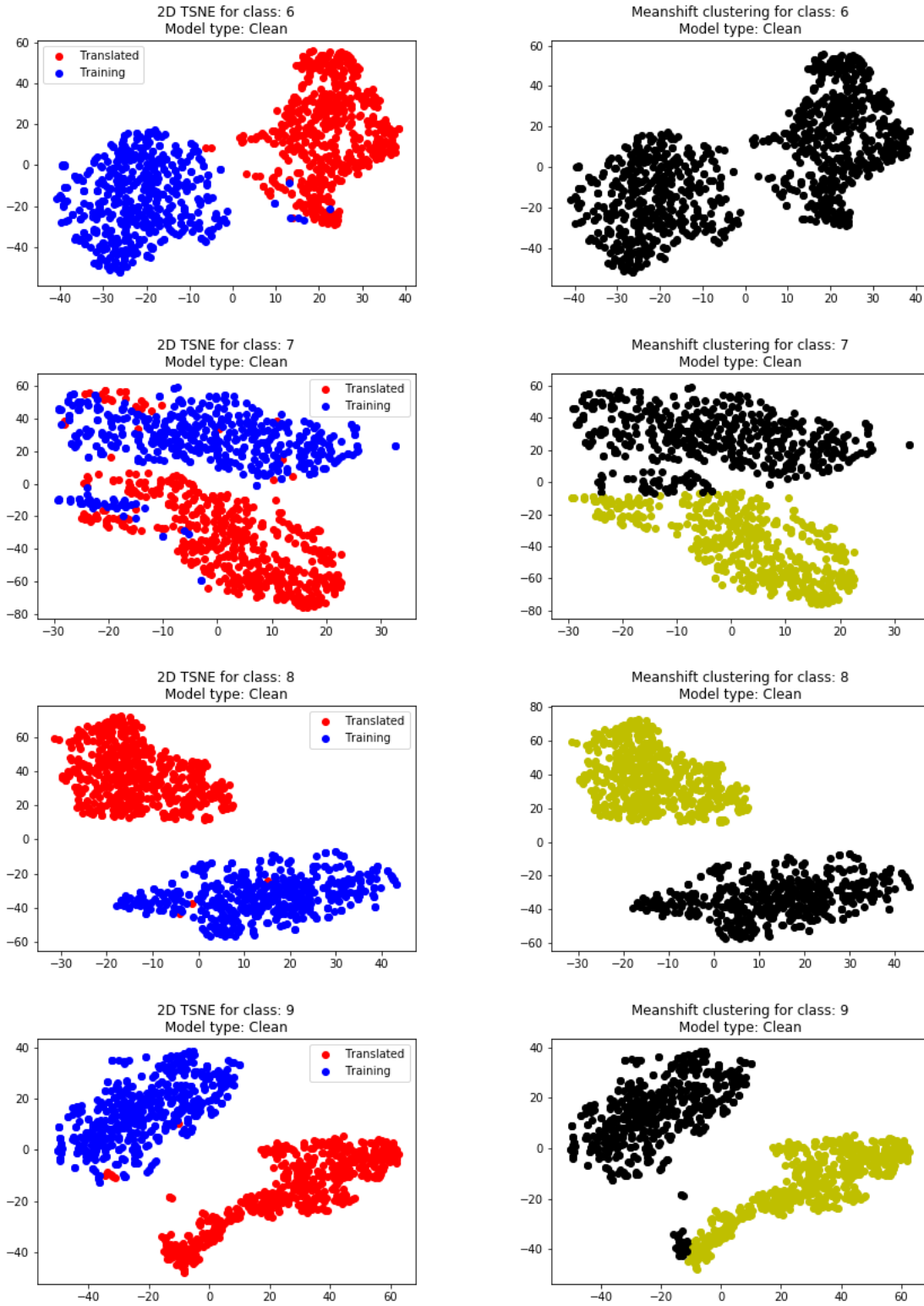
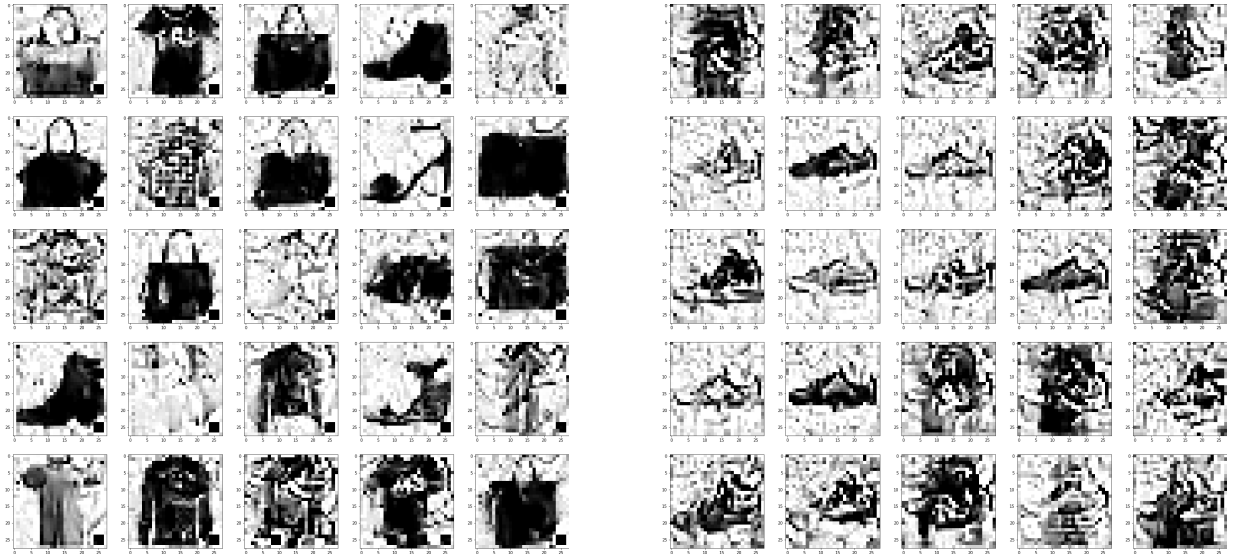


Figure 34. Feature representation clusters for backdoored MNIST models (Clean) with target class 7. Showing class 6 to 9 in this figure. The left column shows the feature representations of the translated and the training images, whereas the right column shows the result of the Mean shift clustering on the corresponding points where different colours represent different classes.



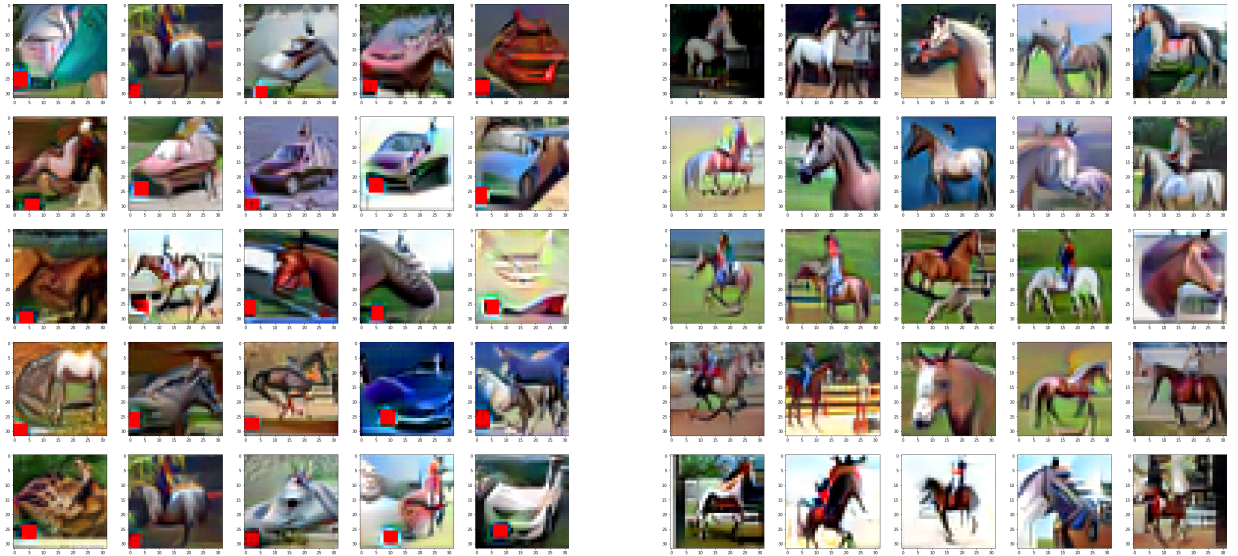
(a) Translated images associated with the poisoned data (b) Translated images associated with the training data

Figure 35. Image in clusters for backdoored Fashion-MNIST models (Localised) with target class *Sneaker*. It is important to note that these 25 images are randomly chosen from each cluster.



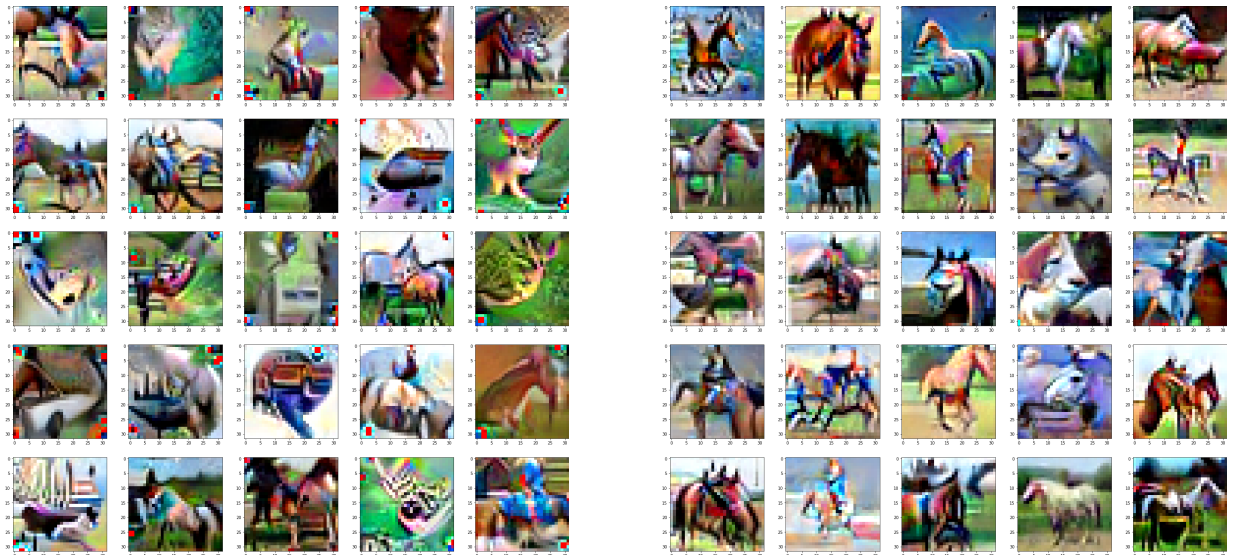
(a) Translated images associated with the poisoned data (b) Translated images associated with the training data

Figure 36. Image in clusters for backdoored Fashion-MNIST models (Distributed) with target class *Sneaker*. It is important to note that these 25 images are randomly chosen from each cluster.



(a) Translated images associated with the poisoned data (b) Translated images associated with the training data

Figure 37. Image in clusters for backdoored CIFAR models (Localised) with target class *Horse*. It is important to note that these 25 images are randomly chosen from each cluster.



(a) Translated images associated with the poisoned data (b) Translated images associated with the training data

Figure 38. Image in clusters for backdoored CIFAR models (Distributed) with target class *Horse*. It is important to note that these 25 images are randomly chosen from each cluster.

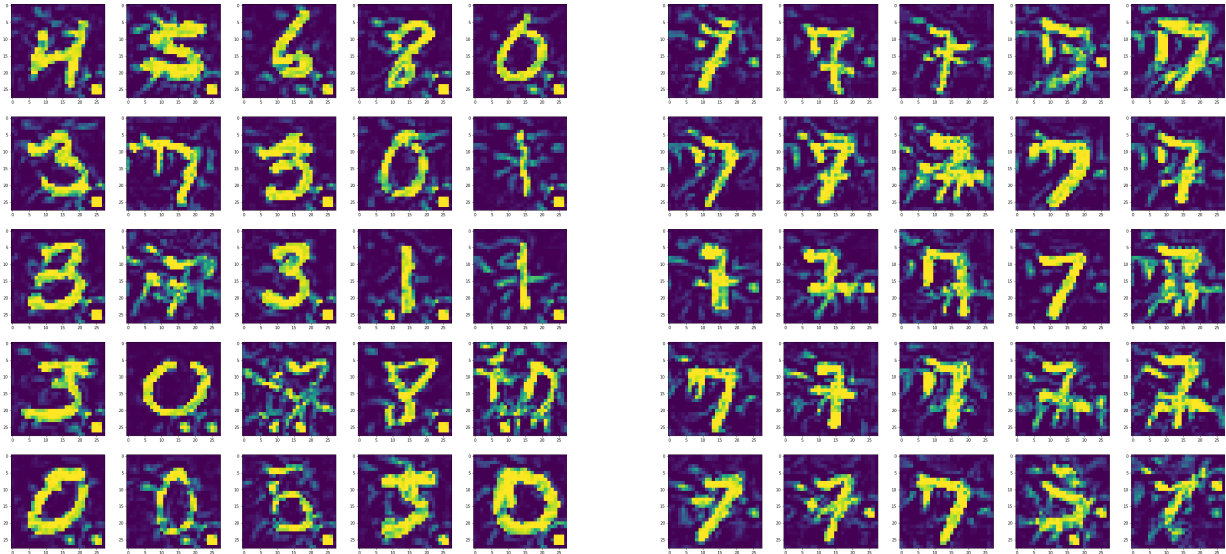


Figure 39. Image in clusters for backdoored MNIST models (Localised) with target class 7. It is important to note that these 25 images are randomly chosen from each cluster.

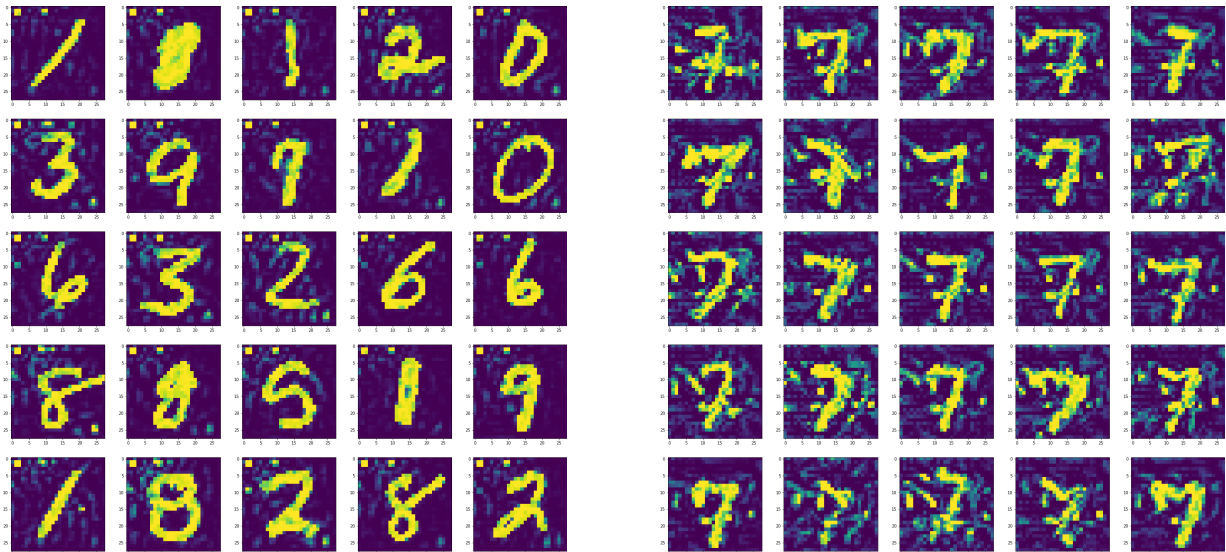


Figure 40. Image in clusters for backdoored MNIST models (Distributed) with target class 7. It is important to note that these 25 images are randomly chosen from each cluster.